

Handwritten scribble

~~CONFIDENTIAL~~

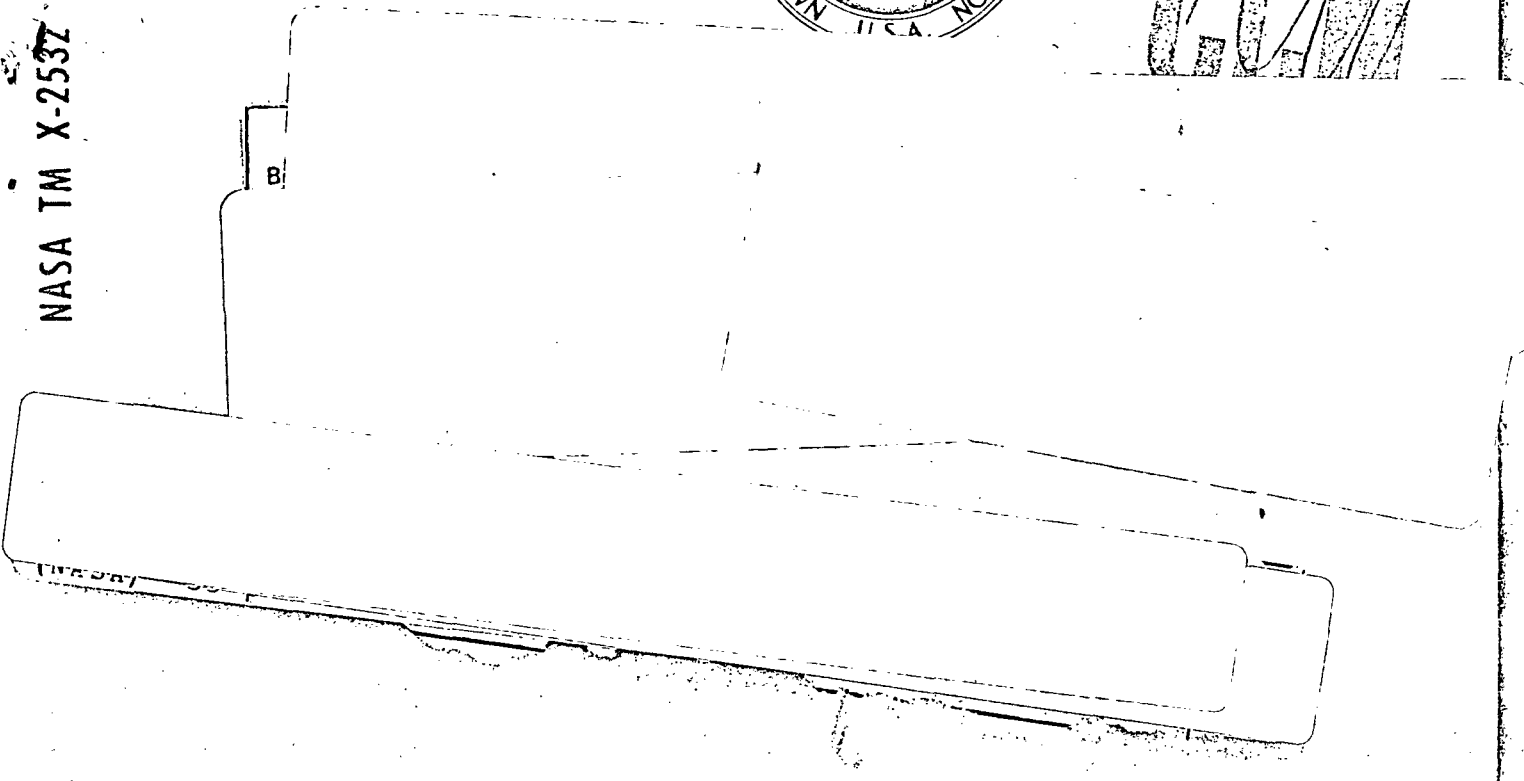
NASA TECHNICAL
MEMORANDUM



NASA TM X-2532

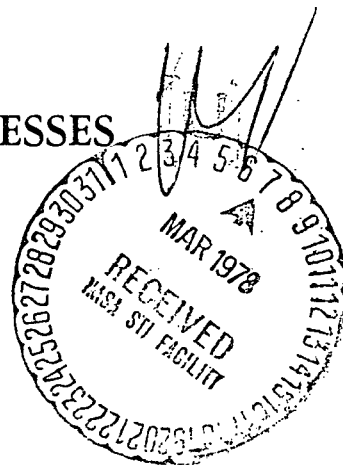
Handwritten: GCM

NASA TM X-2532



AERODYNAMIC CHARACTERISTICS OF
TWO NASA SUPERCRITICAL AIRFOILS
WITH DIFFERENT MAXIMUM THICKNESSES

by *Charles D. Harris*
Langley Research Center
Hampton, Va. 23365



NATIONAL AERONAUTICS AND SPACE ADMINISTRATION • WASHINGTON, D. C. • APRIL 1972

~~CONFIDENTIAL~~

Handwritten: CAT C/

SECRET
The following information was obtained from a confidential source who has provided reliable information in the past. It is being furnished to you for your information only. It is not to be disseminated outside your office.

68-15-878
SEARCHED
SERIALIZED
INDEXED
FILED

RECEIVED
FEDERAL BUREAU OF INVESTIGATION
U. S. DEPARTMENT OF JUSTICE
WASHINGTON, D. C.

THIS PAGE IS UNCLASSIFIED

ERRATA

2/01/95

NASA Technical Memorandum X-2532

AERODYNAMIC CHARACTERISTICS OF TWO NASA SUPERCRITICAL
AIRFOILS WITH DIFFERENT MAXIMUM THICKNESSES

By Charles D. Harris

April 1972

Pages 23 to 35: Section drag coefficients, c_d , for the 10-percent-thick airfoils shown in figures 7, 8, and 9 are incorrect because of an erroneous instrumentation sensitivity constant. Correct drag levels are roughly 8 percent greater than indicated. Discussion and conclusions pertaining to these figures are unaffected.

Issued August 1973

THIS PAGE IS UNCLASSIFIED

07-27-1335

~~CONFIDENTIAL~~

1. Report No. NASA TM X-2532	2. Government Accession No.	3. Recipient's Catalog No.
4. Title and Subtitle AERODYNAMIC CHARACTERISTICS OF TWO NASA SUPER-CRITICAL AIRFOILS WITH DIFFERENT MAXIMUM THICKNESSES (U)	5. Report Date April 1972	6. Performing Organization Code
	8. Performing Organization Report No. L-8173	10. Work Unit No. 742-73-01-14
7. Author(s) Charles D. Harris	9. Performing Organization Name and Address NASA Langley Research Center Hampton, Va. 23365	11. Contract or Grant No.
12. Sponsoring Agency Name and Address National Aeronautics and Space Administration Washington, D.C. 20546	13. Type of Report and Period Covered Technical Memorandum	14. Sponsoring Agency Code

15. Supplementary Notes

16. Abstract

Wind-tunnel tests have been conducted at Mach numbers from 0.60 to 0.81 on two supercritical airfoils with maximum thicknesses of 10 and 11 percent of the chord. The results demonstrate the influence of variations in certain airfoil shape parameters and provide a source of systematic experimental data for the supercritical airfoil.

CLASSIFICATION CHANGE
UNCLASSIFIED

To NASA Langley Research Center
By authority of NASA Langley Research Center Date 6/10/76
Changed by D. Stueckelmann Date 11/4/76
Classified Document Master Control Station, NASA
Scientific and Technical Information Facility

~~CLASSIFIED BY IT 20254 (10/3/72) NAC-2431~~
~~SUBJECT TO GENERAL DECLASSIFICATION~~
~~SCHEDULE OF EXECUTIVE ORDER 11652.~~
~~AUTOMATICALLY DOWNGRADED AT~~
~~TWO-YEAR INTERVALS.~~
~~DECLASSIFIED ON DECEMBER 31, 1978~~

17. Key Words (Suggested by Author(s)) Supercritical airfoils Transonic aerodynamics	18. Distribution Statement Confidential Available to U.S. Government Agencies and Their Contractors Only
--	--

19. Security Classif. (of this report) Confidential Group 4	20. Security Classif. (of this page) Unclassified	21. No. of Pages 55	22. Price
GROUP 4 Downgraded at two-year intervals; Declassified after 12 years		This material contains information affecting the national defense of the United States within the meaning of the espionage laws, Title 18, U.S.C., Secs. 793 and 794, the transmission or revelation of which in any manner to an unauthorized person is prohibited by law.	

~~CONFIDENTIAL~~

~~CONFIDENTIAL~~

AERODYNAMIC CHARACTERISTICS OF TWO NASA SUPERCRITICAL AIRFOILS WITH DIFFERENT MAXIMUM THICKNESSES*

By Charles D. Harris
Langley Research Center

SUMMARY

Wind-tunnel tests have been conducted at Mach numbers from 0.60 to 0.81 to determine the aerodynamic characteristics of two NASA supercritical airfoils with maximum thicknesses of 10 and 11 percent of the chord. Other geometric dissimilarities were present which would prevent a direct comparison of the two airfoils, but the results provide a source of systematic experimental data for the supercritical airfoil.

For the thinner airfoil, stall (onset of trailing-edge separation) begins at an approximately 0.1 higher normal-force coefficient at the higher test Mach numbers, and the drag divergence Mach number at a normal-force coefficient of 0.7 was 0.01 higher. Both effects are associated with lower induced velocities over the thinner airfoil.

INTRODUCTION

In principle, the NASA supercritical airfoil (refs. 1 to 4) is shaped to reduce the drag associated with energy losses due to shock waves and flow separation. It was conceived to have extensive regions of local supersonic flow over the upper surface but have only weak shock waves near the trailing edge; thus, satisfactory performance characteristics were maintained well beyond the critical Mach number (the free-stream Mach number at which the local velocity becomes sonic at some point on the airfoil).

This report documents results of an early phase of the supercritical airfoil wind-tunnel development program involving comparisons of two supercritical airfoils with maximum thicknesses of 10 and 11 percent of the chord. Although maximum thickness was the primary variable between the two airfoils, other geometric dissimilarities were present which would prevent a direct comparison. The results are useful, however, in demonstrating the effects of variations in certain airfoil shape parameters and provide a further source of systematic experimental data for the supercritical airfoil.

The wind-tunnel results presented herein for Mach numbers from 0.60 to 0.81 were obtained in the Langley 8-foot transonic pressure tunnel. Normal-force, drag, and

* Title, Unclassified

~~CONFIDENTIAL~~

pitching-moment coefficients were determined from static-pressure measurements along the surface of the airfoil and total-pressure measurements in the wake of the model.

SYMBOLS

- C_p pressure coefficient, $\frac{p_l - p_\infty}{q_\infty}$
- $C_{p,sonic}$ pressure coefficient corresponding to local Mach number of 1.0
- c chord of airfoil, centimeters (inches)
- c_d section drag coefficient, $\sum c'_d \frac{\Delta z}{c}$
- c'_d point drag coefficient (ref. 5)
- c_m section pitching-moment coefficient about the quarter-chord point,
$$\sum_{l.s.} C_p \frac{\Delta x}{c} \left(0.25 - \frac{x}{c}\right) - \sum_{u.s.} C_p \frac{\Delta x}{c} \left(0.25 - \frac{x}{c}\right)$$
- c_n section normal-force coefficient, $\sum_{l.s.} C_p \frac{\Delta x}{c} - \sum_{u.s.} C_p \frac{\Delta x}{c}$
- M Mach number
- m slope of airfoil surface, $\frac{dy}{dx}$
- p static pressure, newtons per meter² (pounds per foot²)
- q dynamic pressure, newtons per meter² (pounds per foot²)
- R Reynolds number based on chord of 10-percent-thick airfoil, 63.5 centimeters (25.0 inches)
- r airfoil leading-edge radius, centimeters (inches)
- t airfoil thickness, centimeters (inches)

- x ordinate along airfoil reference line measured from airfoil leading edge, centimeters (inches)
- y ordinate normal to airfoil reference line, centimeters (inches)
- z vertical distance in wake profile measured from top of rake, centimeters (inches)
- α angle of attack of airfoil reference line, degrees

Subscripts:

- l conditions at local point on airfoil
- max maximum
- te trailing edge
- ∞ conditions in undisturbed stream

Abbreviations:

- l.s. airfoil lower surface
- u.s. airfoil upper surface

APPARATUS AND TECHNIQUES

The apparatus and testing techniques used during this investigation were the same as those described in references 1 and 2. These descriptions are repeated herein for convenience. A number of previous papers have discussed the design philosophy of the supercritical airfoil concept (refs. 1 and 2, for example), and these discussions are not repeated herein.

Wind Tunnel

The investigation was conducted in the Langley 8-foot transonic pressure tunnel. This tunnel is a single-return, rectangular wind tunnel with controls that allow for the independent variation of Mach number, stagnation pressure, temperature, and dewpoint (ref. 6). The upper and lower walls of the test section are axially slotted to permit

testing through the transonic speed range. The total slot width at the position of the model averaged about 5 percent of the width of the upper and lower walls.

The solid side walls and slotted upper and lower walls make this tunnel well suited to the investigation of two-dimensional models since the side walls act as end plates while the slots permit development of the flow field in the vertical direction.

Models

Airfoil number designations used are those assigned as part of the numbering system for the overall supercritical airfoil development program.

Models of two supercritical airfoils (fig. 1), each having a thickness-chord ratio at the blunt trailing edge of 0.01 (trailing-edge thickness 1 percent of the chord), were used in this investigation. The trailing-edge thickness was somewhat greater than that shown to be desirable in reference 2, but this should not invalidate conclusions drawn from the data presented herein. Coordinates and surface slopes of the two airfoils are presented in tables I and II and the chordwise distribution of surface slopes is presented graphically in figure 2.

The 11 percent-thick $((t/c)_{\max} = 0.11)$ airfoil (airfoil 5) was derived from an earlier airfoil with sharp trailing edge (airfoil 4) by rotating the rear lower surface downward about the 64-percent-chord line to the desired trailing-edge thickness. (Airfoils 4 and 5 are compared and discussed in ref. 2.)

The 10 percent-thick $((t/c)_{\max} = 0.10)$ airfoil (airfoil 9), considered to be more representative of the midsemispan section thicknesses used on present-day transports, had a smaller leading-edge radius and increased rear camber (fig. 1). Figure 2(a) indicates slightly reduced curvature around the 50-percent-chord station and increased curvature over approximately the rearmost 25 percent of the upper surface of the airfoil for the 10-percent-thick airfoil. (For small values of slope, curvature may be closely approximated by the second derivative of the airfoil contour, d^2y/dx^2 .)

The airfoil models were mounted in an inverted position and completely spanned the width of the tunnel. Angle of attack was changed manually by rotating the model about pivots in the tunnel sidewalls. Sketches of airfoil 9 and the profile drag rake are presented in figure 3, and a photograph of one of the airfoils and the profile drag rake mounted in the tunnel is shown as figure 4.

Boundary-Layer Transition

Based on the technique discussed in reference 7, transition strips were applied along the 23-percent-chord line on both the upper and lower surfaces to simulate full-scale Reynolds number boundary-layer characteristics at the trailing edge as well as full-scale

shock-wave positions. The simulation is limited on the upper surface to those conditions in which the shock wave occurs behind the transition, that is, to the higher test Mach numbers. Full-scale simulation on the lower surface would be valid through the Mach number range of the investigation since laminar flow can be maintained ahead of the trip for all conditions. The transition strips consisted of 0.25-cm-wide (0.10 in.) bands of No. 90 carborundum grains.

Caution should be exercised when comparing the present results with results from earlier supercritical airfoil investigations since transition grit size and locations used during earlier phases of the supercritical development program differed from those just described.

Measurements

Surface pressure measurements.- Normal forces and pitching moments acting on the airfoils were determined from surface static-pressure measurements. The surface pressures were obtained from chordwise rows of orifices located approximately 0.28c from the tunnel center line on airfoil 5 and 0.32c from the tunnel center line on airfoil 9. The maximum range of the transducers in the differential pressure-scanning values used to measure the static pressure at the surface was $\pm 68.9 \text{ kN/m}^2$ ($\pm 10 \text{ lb/in}^2$). The orifices were concentrated near the leading and trailing edges of the airfoils to define the severe pressure gradients in these regions. In addition, a rearward-facing orifice was included in the trailing edge of the 10-percent-thick airfoil (airfoil 9).

Wake measurements.- Drag forces acting on the airfoils, as measured by the momentum deficiency within the wake, were derived from vertical variations of the total and static pressures measured across the wake with the profile drag rake shown in figure 3(b). The rake was positioned in the vertical center-line plane of the tunnel, approximately 1 chord length rearward of the trailing edge of the airfoil. The total-pressure tubes were flattened horizontally and closely spaced vertically (0.36 percent of the airfoil chord) in the region of the wake associated with skin-friction boundary-layer losses. Outside this region, the tube vertical spacing progressively widened until, in the region above the wing where only shock losses were anticipated, the total-pressure tubes were spaced about 7.3 percent chord apart. Static-pressure tubes were distributed as shown in figure 3(b). The rake was attached to the conventional center-line sting mount of the tunnel which permitted it to be moved vertically to center the close concentration of tubes on the boundary-layer wake.

Total and static pressures across the wake were also measured with the use of differential pressure-scanning values. The maximum range of the transducer in the valve connected to total-pressure tubes intended to measure boundary-layer losses was

$\pm 34.5 \text{ kN/m}^2$ ($\pm 5 \text{ lb/in}^2$); the corresponding maximum range for measuring shock losses and static pressure was $\pm 6.9 \text{ kN/m}^2$ ($\pm 1 \text{ lb/in}^2$).

Reduction of Data

Calculation of c_n and c_m . - Section normal-force and pitching-moment coefficients were obtained by numerical integration (based on the trapezoidal method) of the local surface pressure coefficient measured at each orifice multiplied by an appropriate weighting factor (incremental area).

Calculation of c_d . - To obtain section drag coefficients from the total and static pressures behind the model, point drag coefficients for each of the total-pressure measurements were computed by using the procedure of reference 5. These point drag values were again summed by numerical integration across the wake based on the trapezoidal method.

Wind-Tunnel Wall Effects

The major interference effect of the wind-tunnel walls was an upflow at the inverted model. This upflow, proportional to the normal-force coefficient, results in the measured geometric angle of attack being significantly greater than the aerodynamic angle of attack at the higher normal-force coefficients. The mean value of this upflow (in degrees) at the midchord of the model may be estimated by the theory of reference 8 to be approximately 3 times the section normal-force coefficient. Based on experience in other two-dimensional tests in the Langley 8-foot transonic pressure tunnel, however, such a correction is believed to be unrealistically large. Because of this uncertainty, the uncorrected geometric angles of attack are used in the results presented herein.

The theory of reference 8 also indicates that tunnel blockage effects would be small; consequently, no corrections have been applied to the data to account for blockage effects.

TEST CONDITIONS

Tests were conducted at Mach numbers from 0.60 to 0.81 at a stagnation pressure of 0.1013 MN/m^2 (1 atm). Wind-tunnel Reynolds numbers corresponding to these conditions and based on the chord of airfoil 9 (63.5 cm (25.0 in.)) varied as shown in figure 5. The stagnation temperature of the tunnel air was automatically controlled at approximately 322 K (120° F) and the air was dried until the dewpoint in the test section was reduced sufficiently to avoid condensation effects.

~~CONFIDENTIAL~~

PRESENTATION OF RESULTS

Section force and moment coefficients of the 11-percent-thick airfoil (airfoil 5) are presented over an extensive angle-of-attack range in figure 6. Data are not available for the 10-percent-thick airfoil with the blunt trailing edge (airfoil 9 as described herein) over an angle-of-attack range as extensive as that for airfoil 5. Data are available (ref. 2) however, on an airfoil with the same section coordinates as airfoil 9 but with a cavity in the trailing edge (airfoil 9a). Since the effect of the cavity on the aerodynamic characteristics is not large, the aerodynamic characteristics of airfoil 9a presented in figure 7 provide a good approximation of the characteristics of airfoil 9. Figure 8 presents a direct comparison between the aerodynamic characteristics of airfoils 5 (11 percent thick) and 9 (10 percent thick) over an abbreviated angle-of-attack range around those at which the design normal-force coefficient for airfoil 9 of 0.7 occurs. The drag-rise characteristics are summarized for a normal-force coefficient of 0.7 in figure 9 and chordwise pressure profiles of the two airfoils are compared in figures 10 and 11.

DISCUSSION

Aside from the difference in maximum thickness, other geometric dissimilarities were present which would prevent a direct, detailed comparison of the two airfoils solely on the basis of differences in maximum thickness. However, general observations concerning the results can be made.

Section Characteristics

Immediately apparent in figure 8 is a substantial increase in normal-force coefficient for the 10-percent-thick airfoil when compared with the 11-percent-thick airfoil at the same angle of attack. The slope of the normal-force curve was not greatly affected. More significantly, however, at the higher test Mach numbers ($M = 0.78$ to 0.81), the normal-force coefficients at which the thinner airfoil begins to stall (manifested by an abrupt increase in the drag level) is approximately 0.1 beyond those at which the 11-percent-thick airfoil begins to stall; thus, a design normal-force coefficient of 0.7 is permitted for the 10-percent-thick airfoil compared with about 0.6 for the 11-percent-thick airfoil. (See also figs. 6 and 7.) Although referred to as stall, separation onset would be a more descriptive term since there is not a sudden large loss of lift but a gradual stall beginning at the trailing edge (rear separation) and reflected as merely a change in the slope of the curve of normal force as a function of angle of attack. The abrupt increase in drag at a particular Mach number was also due in part to increased wave

~~CONFIDENTIAL~~

losses. (Compare, for example, the pressure profiles for $\alpha = 1.0^\circ$ and 1.5° at $M = 0.79$, figs. 10(o) and 10(p).)

Figure 9 shows a drag divergence Mach number roughly 0.01 higher for the thinner airfoil at $c_n = 0.7$. Such an increase in the drag divergence Mach number is consistent with the rule of thumb for conventional airfoils that changes in maximum thickness ratio of 0.01 result in changes in the drag divergence Mach number of approximately 0.01. The higher drag divergence Mach number at $c_n = 0.7$ and the extension of the normal-force coefficient at which stall begins for a particular Mach number are related to the lower induced or perturbation velocities (less negative pressure coefficients) over the thinner airfoil as illustrated in figure 11.

The peak in the drag-rise curve (fig. 9) at $M = 0.78$ was due to the second region of supersonic flow on the upper surface (inherent in the supercritical airfoil concept at intermediate off-design conditions, ref. 4) developing to such an extent that a second shock wave was formed. (See, for example, figs. 10(k) and 10(l).) A reduction of this peak would be achieved by decreasing the trailing-edge thickness (ref. 2).

Pressure Distributions

Lower surface.- The differences in the section characteristics of the two airfoils may be largely identified with the noticeably lower induced velocities (less negative pressure coefficients) over approximately the forward 60 percent of the lower surface on the 10-percent-thick airfoil (fig. 10). These lower induced velocities may be attributed to the reduced curvature of the thinner airfoil in this region (fig. 2).

Although the level of compression on the rear lower surface (referred to as the lower surface cusp) was increased slightly for the 10-percent-thick airfoil, differences in the pressure coefficients in this region were not as noticeable as on the forward region. This was probably because the dissimilarities in curvature over this region were not as pronounced as over the forward region and also because the flow in this region is not as sensitive to small curvature variations.

Upper surface.- The effects on the rear upper surface pressure distribution (fig. 10) associated with the dissimilarities in curvature (fig. 2) rearward of approximately the 60-percent-chord station (reduced curvature around the 50-percent-chord station and increased curvature over approximately the rearmost 25 percent of the chord for the 10-percent-thick airfoil) are increased magnitudes of the second velocity peak (more negative pressure coefficients) and a tendency for the forward shock wave to stabilize at a slightly more forward location at intermediate off-design conditions for the thinner airfoil (figs. 10(l), 10(n), and 10(o), for example). Although the effects associated with these changes in upper surface curvature cannot be completely separated from the influence of

~~CONFIDENTIAL~~

the other geometric differences present, the results are consistent with the trend of the data presented in reference 4 on the effects of changes in rear upper surface curvature.

The upper surface leading-edge velocity peak was considerably higher on the 10-percent-thick airfoil when compared with the 11-percent-thick airfoil at the same angle of attack. If compared at equal values of normal-force coefficient rather than angle of attack, good agreement in leading-edge peak velocities was indicated. (See typical comparison in fig. 11.)

CONCLUDING REMARKS

Wind-tunnel tests have been conducted at Mach numbers from 0.60 to 0.81 to determine the aerodynamic characteristics of two NASA supercritical airfoils with maximum thicknesses of 10 and 11 percent of the chord. This report documents the results of these tests to provide a source of systematic experimental data for the supercritical airfoil. Although maximum thickness was the primary variable, dissimilarities were present which would prevent a direct comparison between the two airfoils. However, general observations concerning the results can be made. For the thinner airfoil, stall (onset of trailing-edge separation) begins at an approximately 0.1 higher normal-force coefficient at the higher test Mach numbers, and the drag divergence Mach number at a normal-force coefficient of 0.7 was 0.01 higher. Both effects are associated with lower induced velocities over the thinner airfoil.

Langley Research Center,
National Aeronautics and Space Administration,
Hampton, Va., March 16, 1972.

~~CONFIDENTIAL~~

REFERENCES

1. Whitcomb, Richard T.; and Clark, Larry R.: An Airfoil Shape for Efficient Flight at Supercritical Mach Numbers. NASA TM X-1109, 1965.
2. Harris, Charles D.: Wind-Tunnel Investigation of Effects of Trailing-Edge Geometry on a NASA Supercritical Airfoil Section. NASA TM X-2336, 1971.
3. Blackwell, James A., Jr.: Aerodynamic Characteristics of an 11-Percent-Thick Symmetrical Supercritical Airfoil at Mach Numbers Between 0.30 and 0.85. NASA TM X-1831, 1969.
4. Harris, Charles D.; and Blackwell, James A., Jr.: Wind-Tunnel Investigation of Effects of Rear Upper Surface Modification on an NASA Supercritical Airfoil. NASA TM X-2454, 1972.
5. Baals, Donald D.; and Mourhess, Mary J.: Numerical Evaluation of the Wake-Survey Equations for Subsonic Flow Including the Effect of Energy Addition. NACA WR L-5, 1945. (Formerly NACA ARR L5H27.)
6. Schaefer, William T., Jr.: Characteristics of Major Active Wind Tunnels at the Langley Research Center. NASA TM X-1130, 1965.
7. Blackwell, James A., Jr.: Preliminary Study of Effects of Reynolds Number and Boundary-Layer Transition Location on Shock-Induced Separation. NASA TN D-5003, 1969.
8. Davis, Don D., Jr.; and Moore, Dewey: Analytical Study of Blockage- and Lift-Interference Corrections for Slotted Tunnels Obtained by the Substitution of an Equivalent Homogeneous Boundary for the Discrete Slots. NACA RM L53E07b, 1953.

~~CONFIDENTIAL~~

TABLE I.- SECTION COORDINATES OF 10-PERCENT-THICK SUPERCRITICAL
AIRFOIL 9 WITH 1-PERCENT-THICK TRAILING EDGE

[c = 63.5 cm (25 in.)]

x/c	Calculated				Experimental	
	y/c		m		y/c	
	Upper	Lower	Upper	Lower	Upper	Lower
0.0075	0.0162	-0.0162	0.850	-0.874	0.0160	-0.0165
.0125	.0196	-.0198	.570	-.610	.0196	-.0201
.0250	.0250	-.0257	.345	-.374	.0250	-.0259
.0375	.0287	-.0297	.255	-.276	.0286	-.0299
.050	.0316	-.0328	.204	-.219	.0314	-.0329
.075	.0359	-.0373	.145	-.153	.0358	-.0374
.100	.0390	-.0406	.110	-.114	.0389	-.0407
.125	.0414	-.0431	.086	-.087	.0415	-.0432
.150	.0434	-.0450	.069	-.067	.0433	-.0451
.175	.0449	-.0465	.056	-.052	.0448	-.0465
.200	.0462	-.0476	.045	-.040	.0461	-.0476
.250	.0480	-.0492	.029	-.021	.0479	-.0491
.300	.0492	-.0499	.017	-.008	.0491	-.0498
.350	.0498	-.0500	.008	.003	.0498	-.0500
.400	.0500	-.0495	.000	.014	.0500	-.0494
.450	.0498	-.0486	-.007	.025	.0499	-.0485
.500	.0493	-.0469	-.013	.042	.0494	-.0468
.550	.0485	-.0442	-.021	.070	.0485	-.0440
.575	.0479	-.0422	-.025	.091	.0480	-.0420
.600	.0472	-.0396	-.029	.120	.0474	-.0393
.625	.0465	-.0362	-.034	.157	.0465	-.0357
.650	.0456	-.0316	-.039	.206	.0456	-.0310
.675	.0445	-.0259	-.046	.239	.0445	-.0255
.700	.0433	-.0202	-.053	.216	.0433	-.0200
.725	.0418	-.0151	-.062	.193	.0419	-.0152
.750	.0402	-.0105	-.073	.169	.0401	-.0109
.775	.0382	-.0066	-.085	.145	.0382	-.0072
.800	.0359	-.0033	-.100	.118	.0359	-.0041
.825	.0332	-.0007	-.118	.089	.0332	-.0014
.850	.0299	.0011	-.140	.056	.0300	.0005
.875	.0261	.0020	-.165	.017	.0264	.0016
.900	.0217	.0019	-.194	-.031	.0220	.0016
.925	.0164	.0004	-.229	-.090	.0167	.0004
.950	.0102	-.0027	-.269	-.164	.0103	-.0026
.975	.0028	-.0079	-.316	-.256	.0035	-.0073
.990	-.0021	-.0123	-.348	-.321	-.0016	-.0120
1.000	-.0057	-.0157	-.370	-.370	-----	-.0157

Leading-edge radius: 0.0212c

~~CONFIDENTIAL~~

~~CONFIDENTIAL~~

TABLE II.- SECTION COORDINATES FOR 11-PERCENT-THICK SUPERCRITICAL
AIRFOIL 5 WITH 1-PERCENT-THICK TRAILING EDGE

[c = 63.0 cm (24.8 in.)]

x/c	y/c		m	
	Upper	Lower	Upper	Lower
0.0065	0.0158	-0.0157	1.000	-1.024
.0125	.0203	-.0206	.612	-.664
.0250	.0267	-.0271	.376	-.414
.0375	.0302	-.0316	.280	-.311
.050	.0334	-.0351	.225	-.244
.075	.0381	-.0403	.161	-.174
.100	.0416	-.0440	.124	-.130
.125	.0444	-.0469	.098	-.100
.150	.0466	-.0491	.080	-.075
.175	.0484	-.0508	.065	-.060
.200	.0499	-.0521	.054	-.047
.250	.0521	-.0539	.036	-.024
.300	.0536	-.0548	.023	-.010
.350	.0545	-.0549	.012	.008
.400	.0548	-.0541	.001	.025
.450	.0549	-.0524	-.006	.043
.500	.0544	-.0497	-.014	.067
.550	.0534	-.0455	-.023	.104
.575	.0529	-.0426	-.028	.131
.600	.0519	-.0389	-.032	.156
.625	.0512	-.0342	-.038	.211
.650	.0502	-.0285	-.044	.244
.675	.0490	-.0224	-.051	.249
.700	.0477	-.0165	-.058	.225
.725	.0461	-.0112	-.067	.201
.750	.0443	-.0065	-.077	.177
.775	.0422	-.0024	-.089	.152
.800	.0398	.0011	-.104	.126
.825	.0370	.0039	-.120	.096
.850	.0338	.0059	-.140	.063
.875	.0300	.0070	-.164	.023
.900	.0256	.0069	-.191	-.026
.925	.0204	.0056	-.223	-.087
.950	.0144	.0024	-.260	-.134
.975	.0074	-.0028	-.302	-.250
1.000	-.0008	-.0108	-.352	-.331

Leading-edge radius: 0.0223c

~~CONFIDENTIAL~~

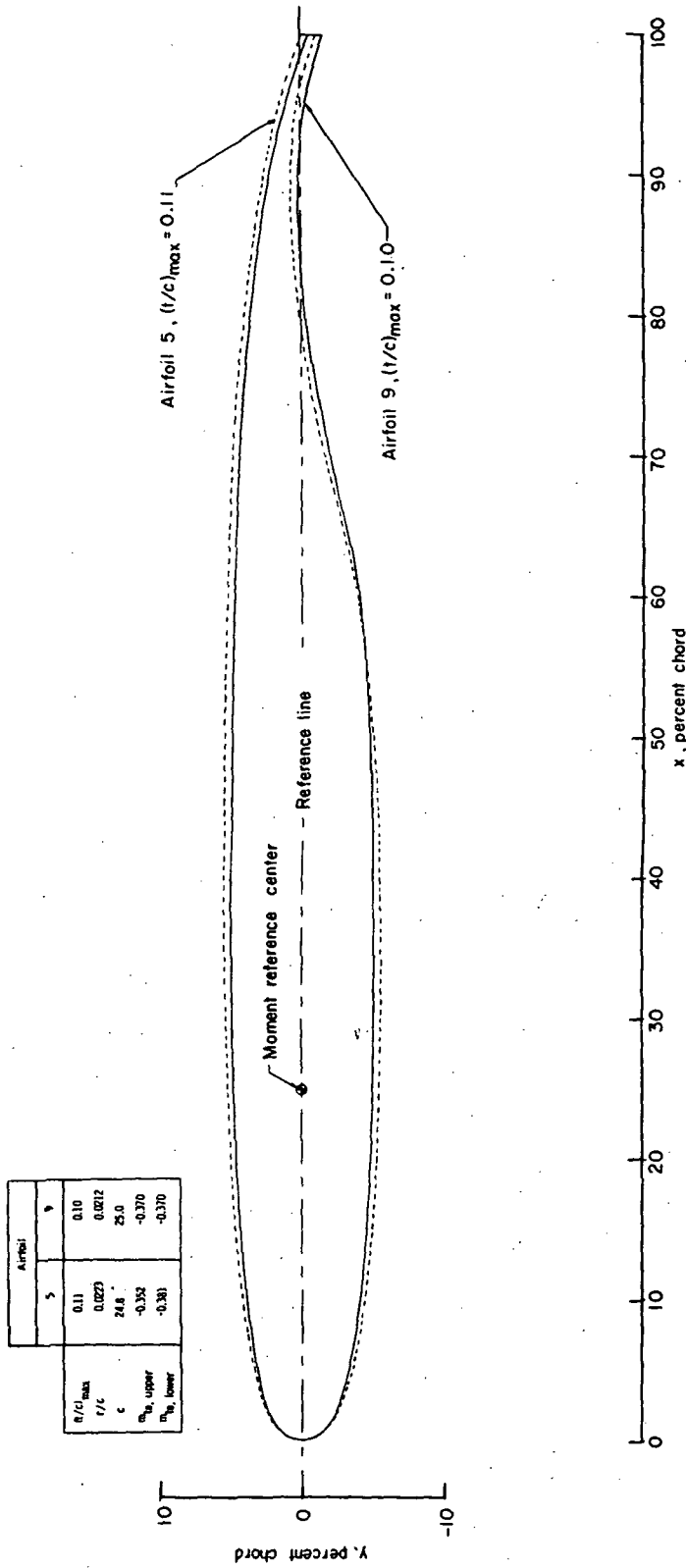
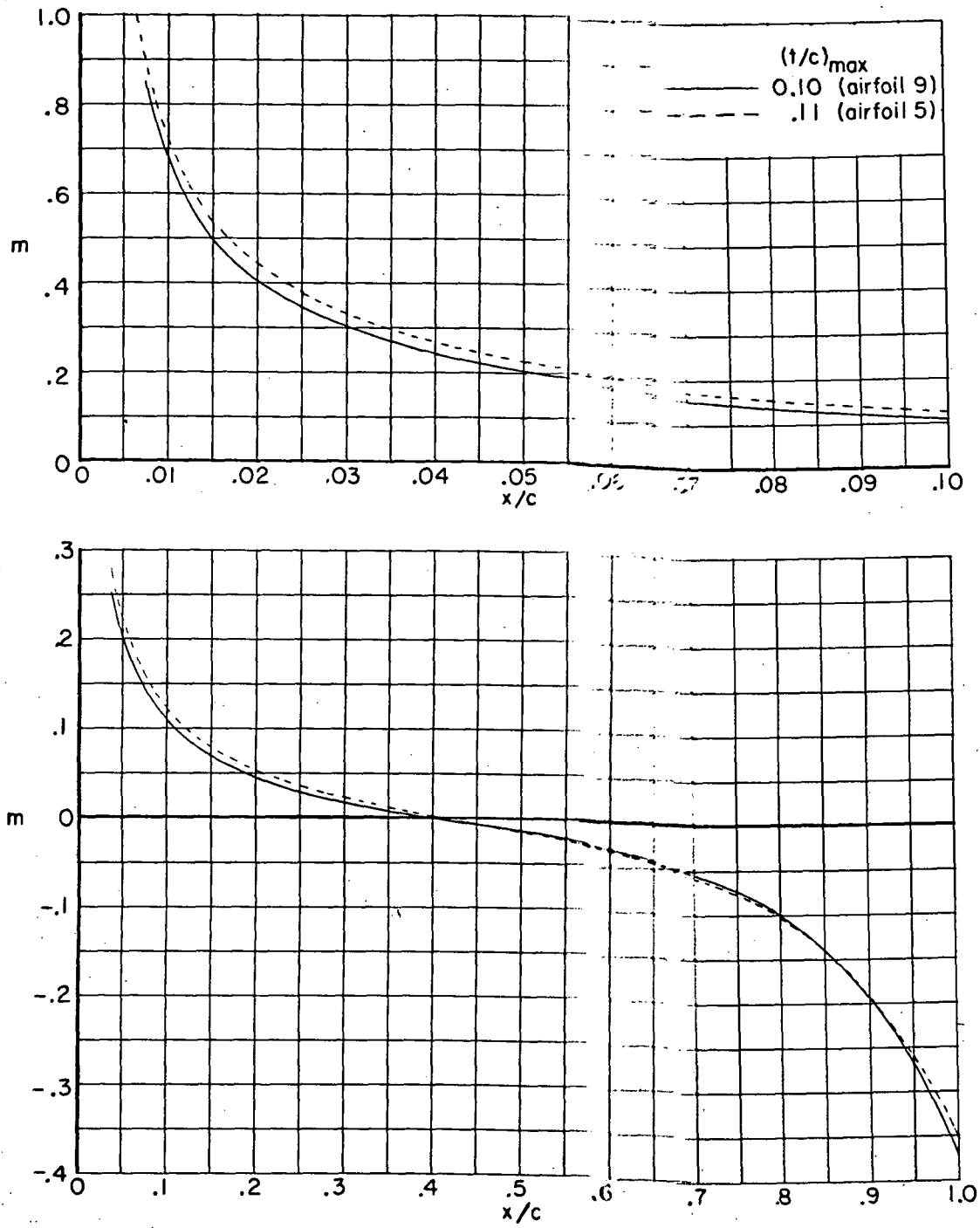


Figure 1.- Airfoil sketches.

~~CONFIDENTIAL~~

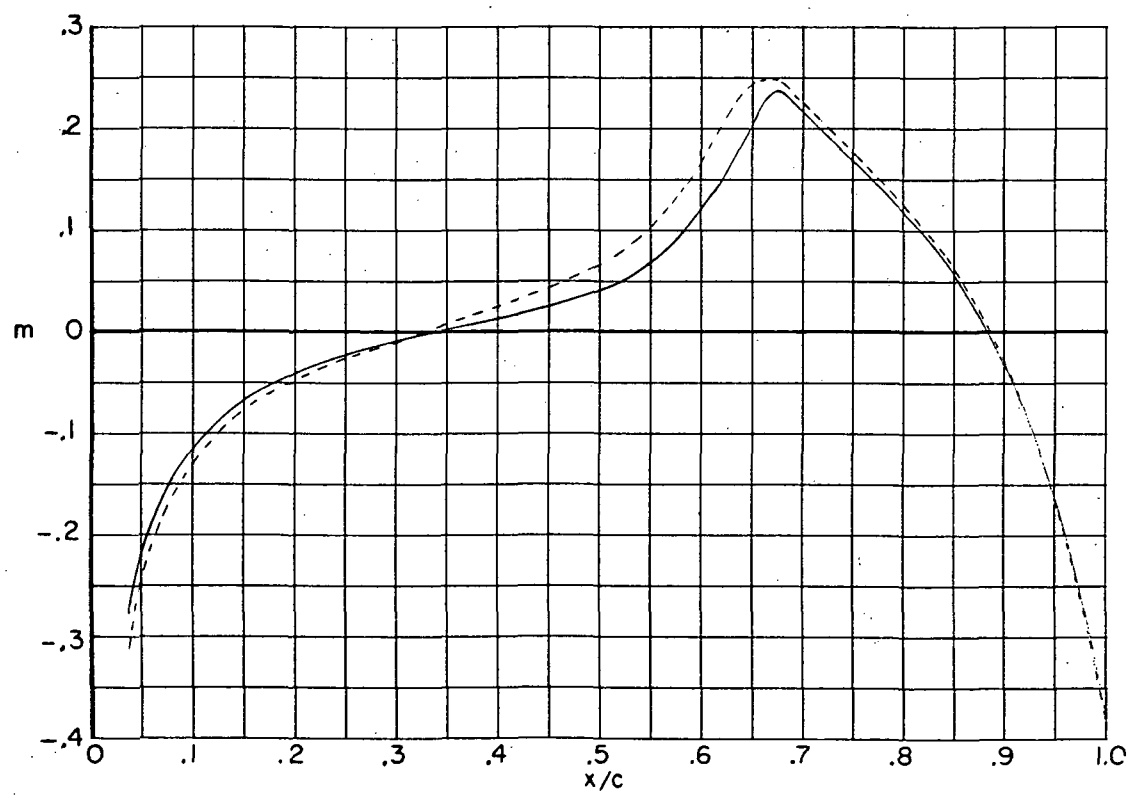
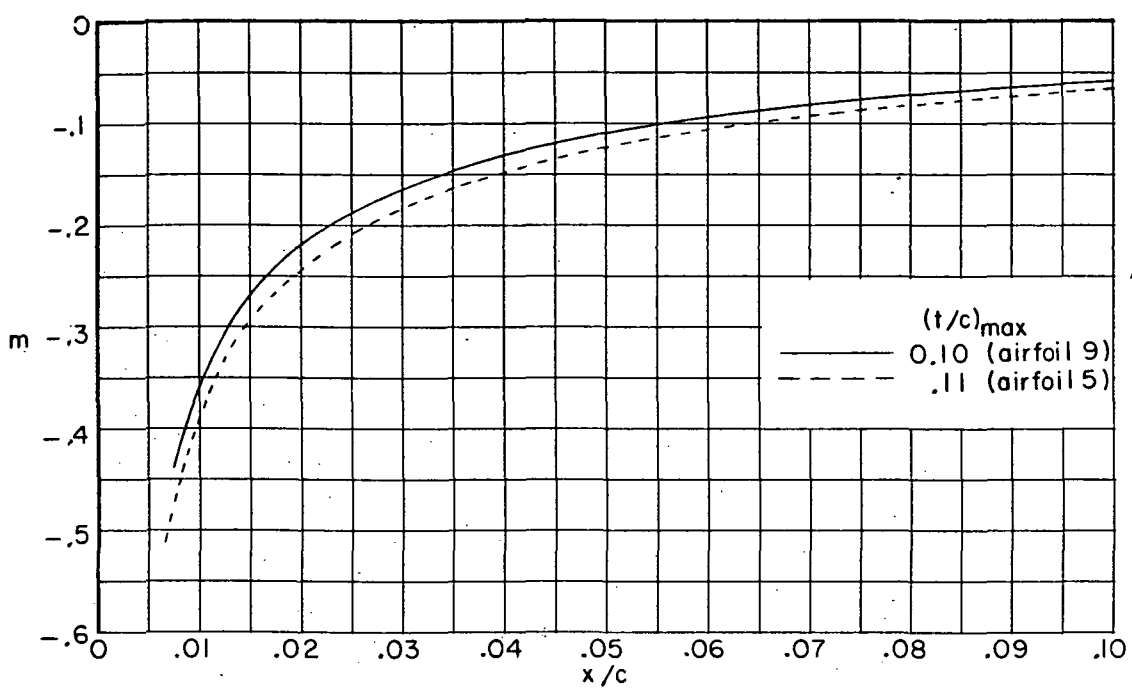


(a) Upper surface,

Figure 2.- Chordwise distribution of airfoil surface slopes.

~~CONFIDENTIAL~~

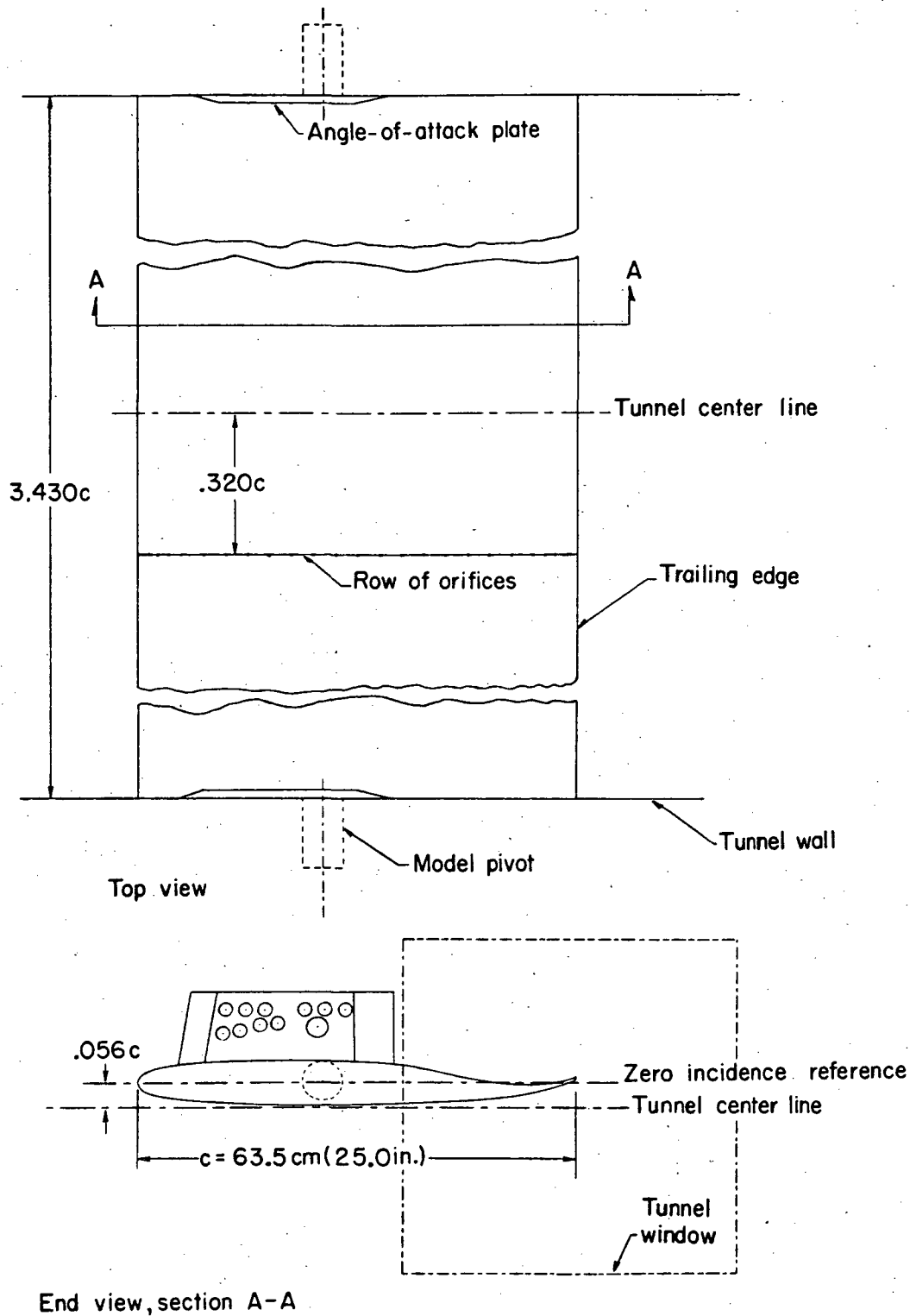
~~CONFIDENTIAL~~



(b) Lower surface.

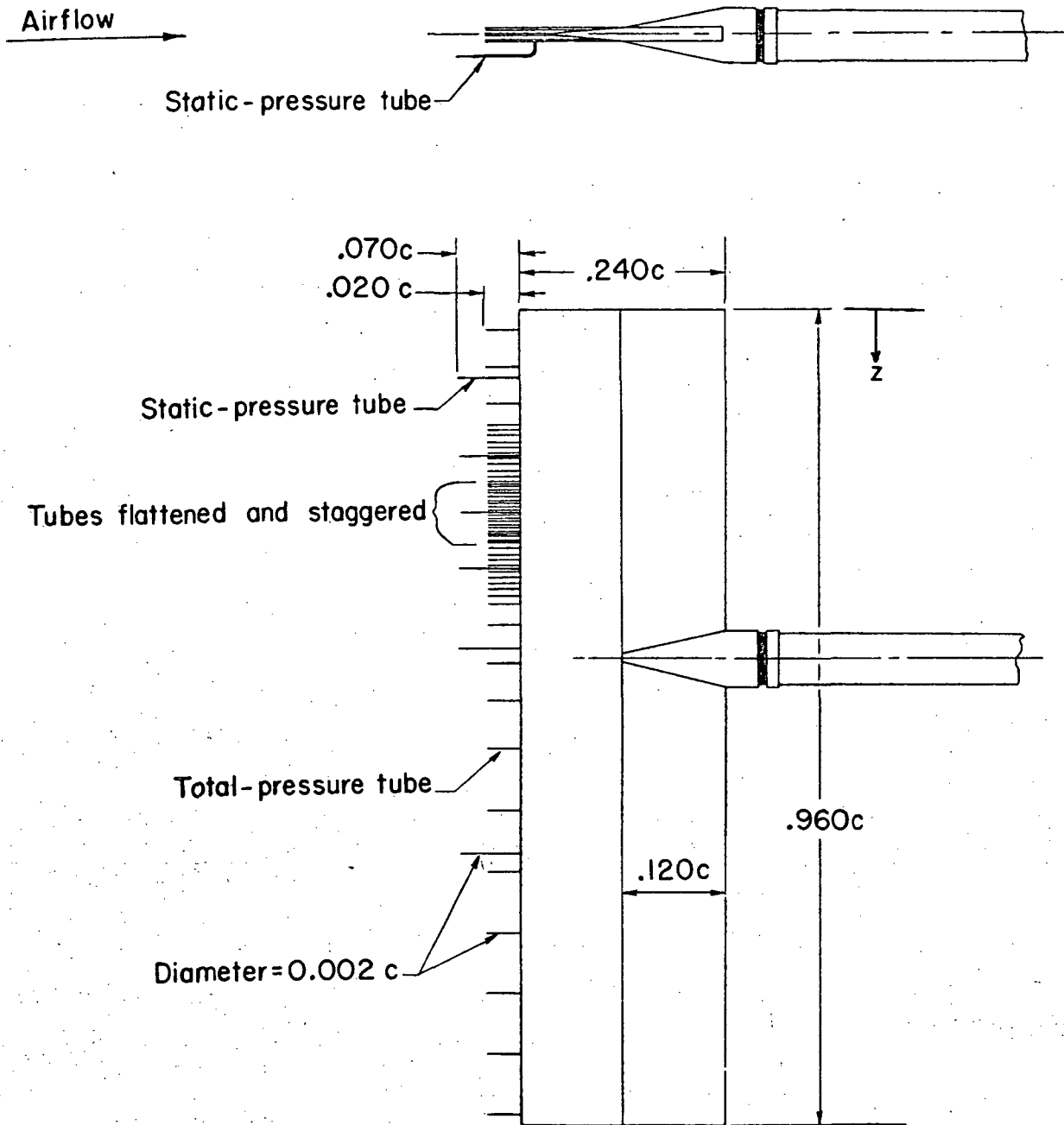
Figure 2.- Concluded.

~~CONFIDENTIAL~~



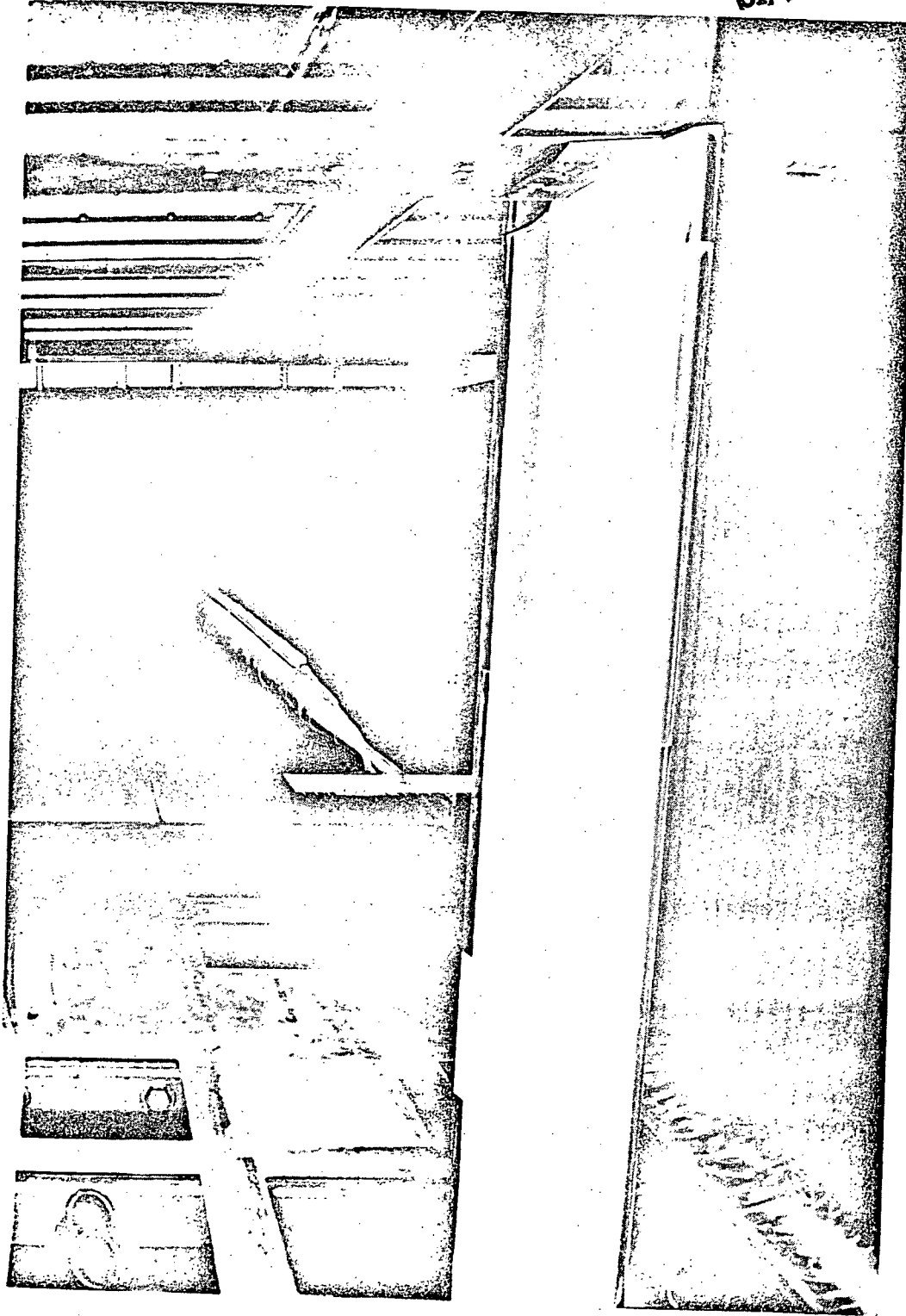
(a) Airfoil 9 mounted in tunnel.

Figure 3.- Apparatus. Dimensions in terms of chord of airfoil 9 ($c = 63.5 \text{ cm (25 in.)}$).



(b) Profile drag rake.
Figure 3.- Concluded.

ORIGINAL PAGE IS
OF POOR QUALITY



L-67-5566

Figure 4.- Supercritical airfoil and profile drag rake in wind tunnel.

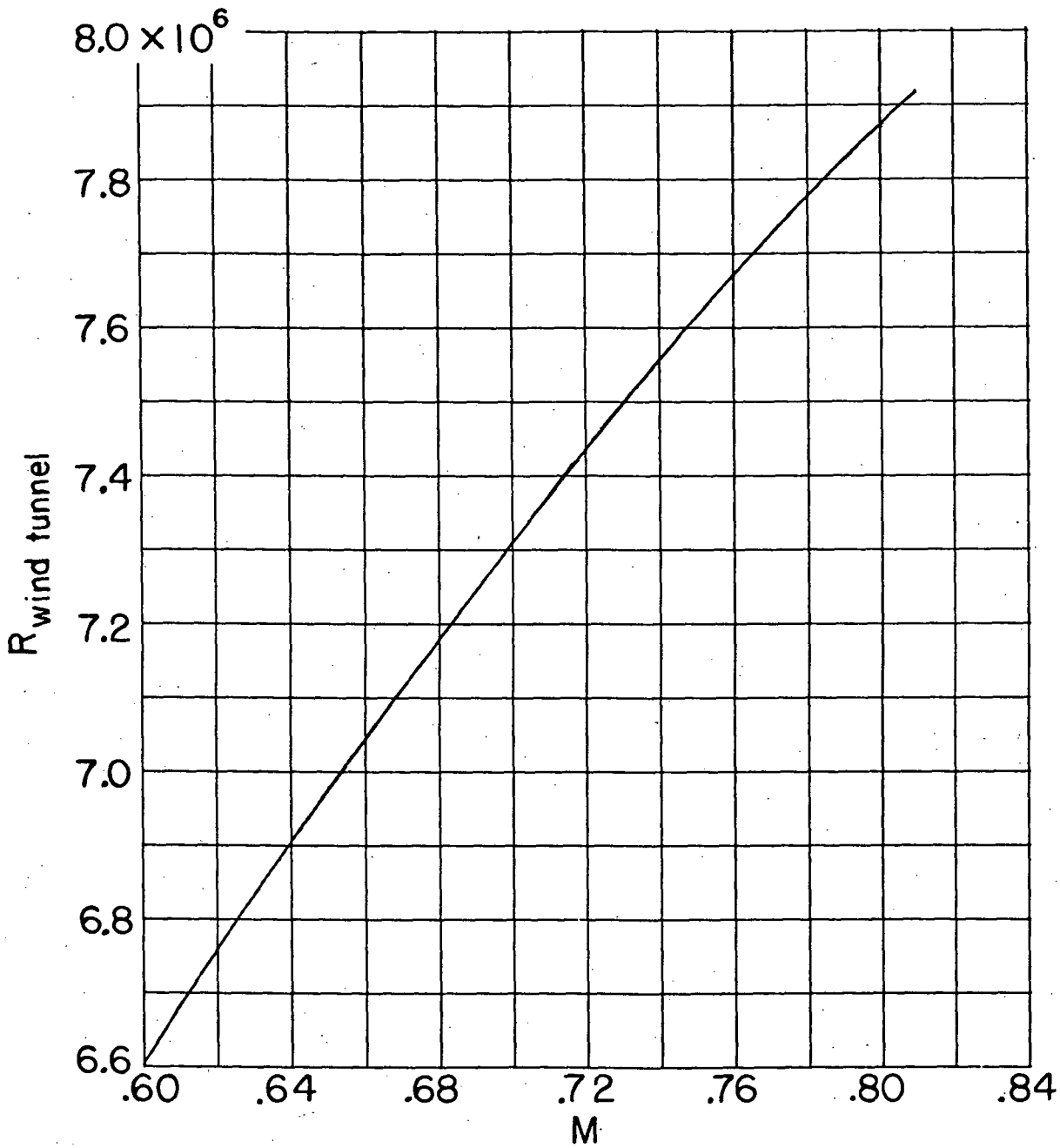


Figure 5.- Variation with Mach number of test wind-tunnel Reynolds number based on chord of airfoil 9 (63.5 cm (25 in.)).

~~CONFIDENTIAL~~

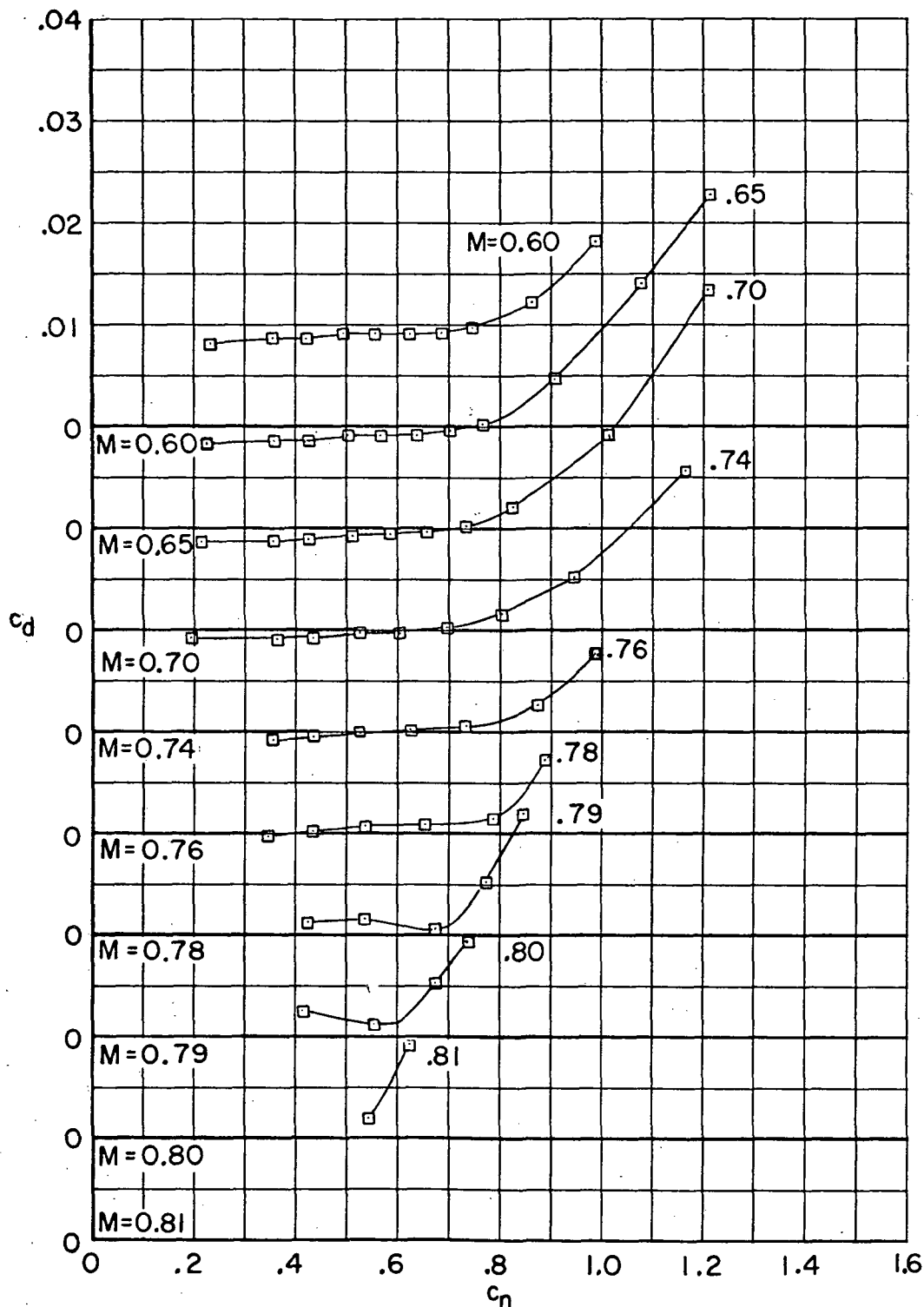


Figure 6. - Variation of section drag coefficient, angle of attack, and section pitching-moment coefficient with section normal-force coefficient at various Mach numbers for 11-percent-thick supercritical airfoil (airfoil 5).

~~CONFIDENTIAL~~

ORIGINAL PAGE IS
OF POOR QUALITY

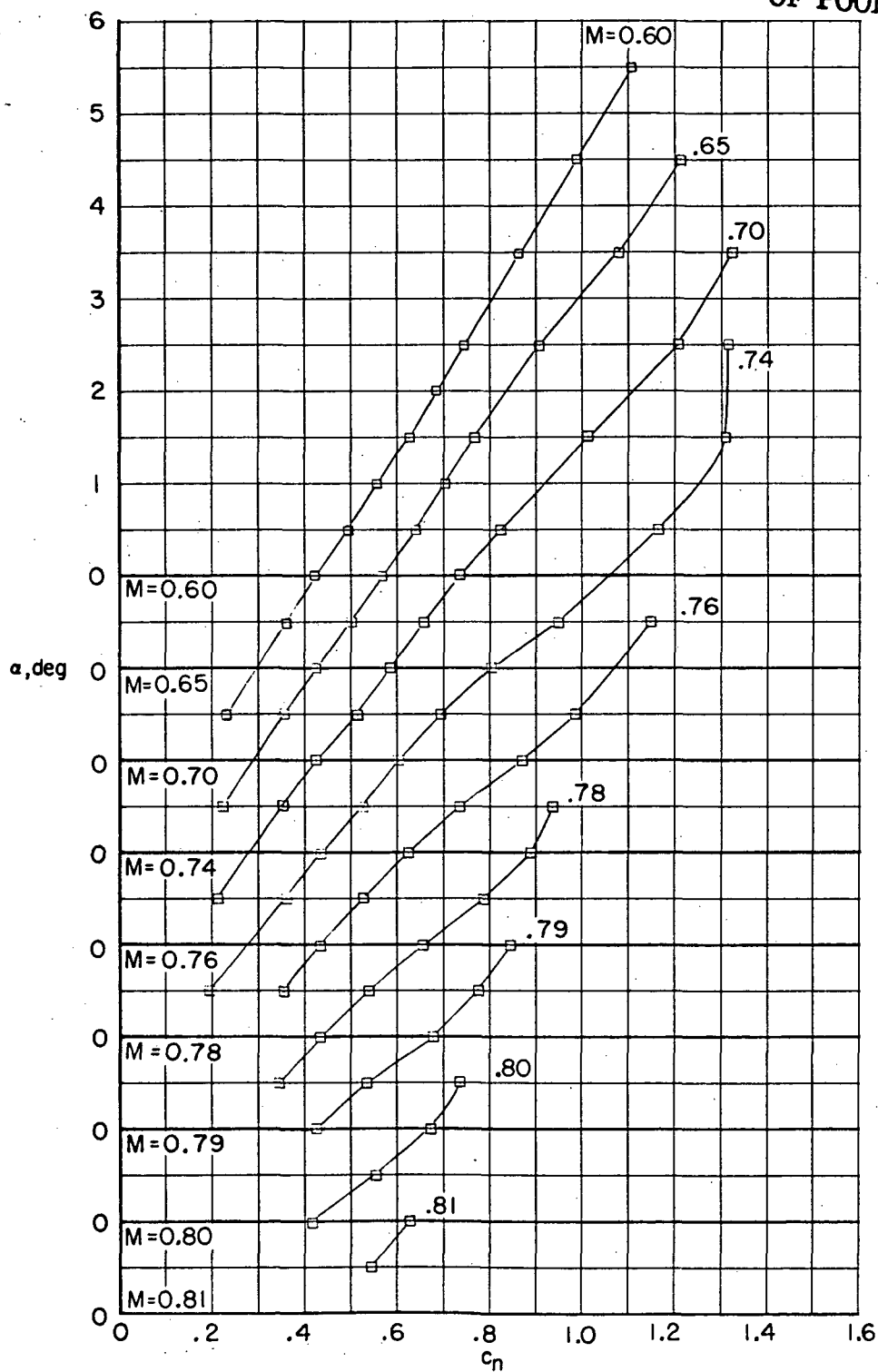


Figure 6.- Continued.

ORIGINAL PAGE IS
OF POOR QUALITY.

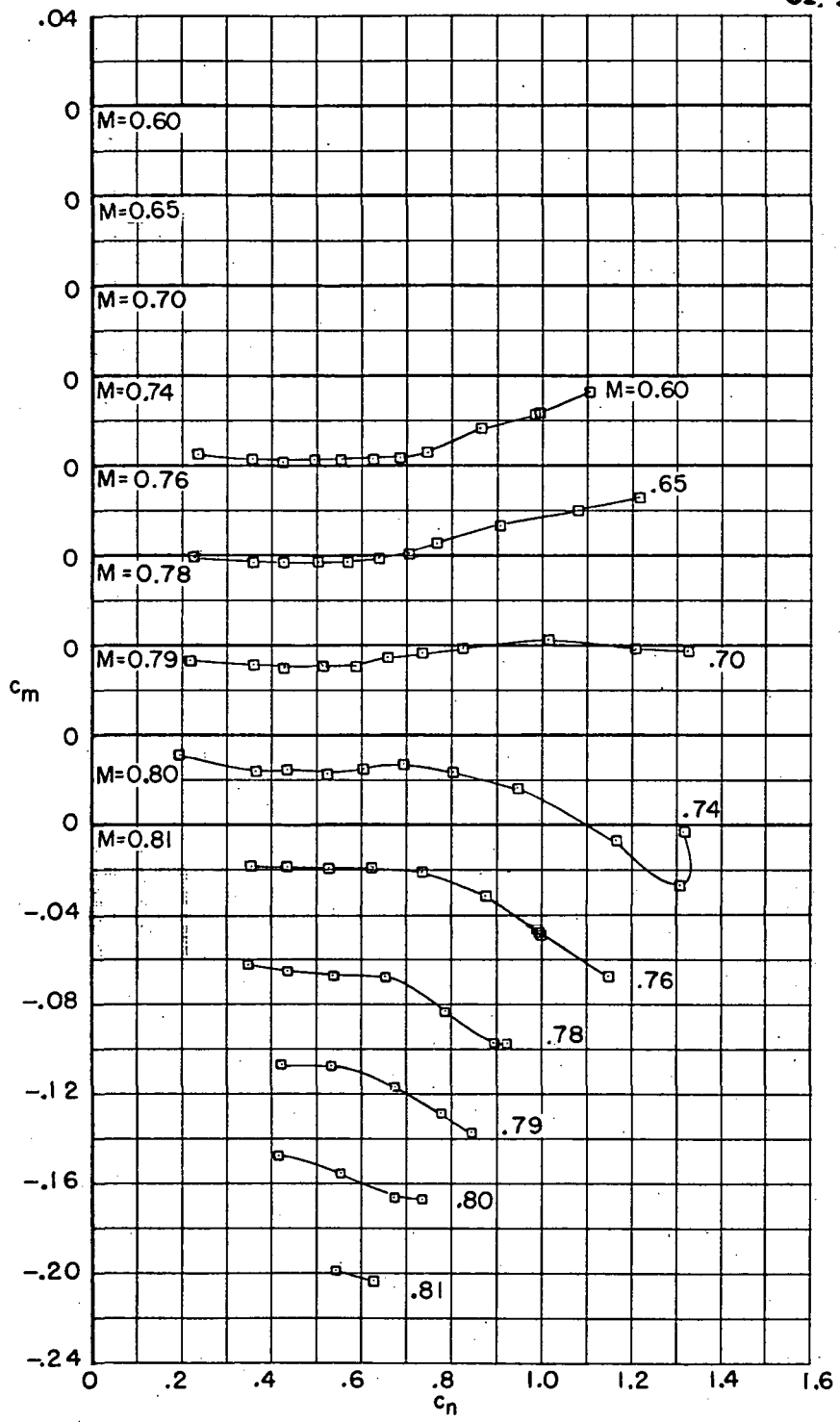


Figure 6.- Concluded.

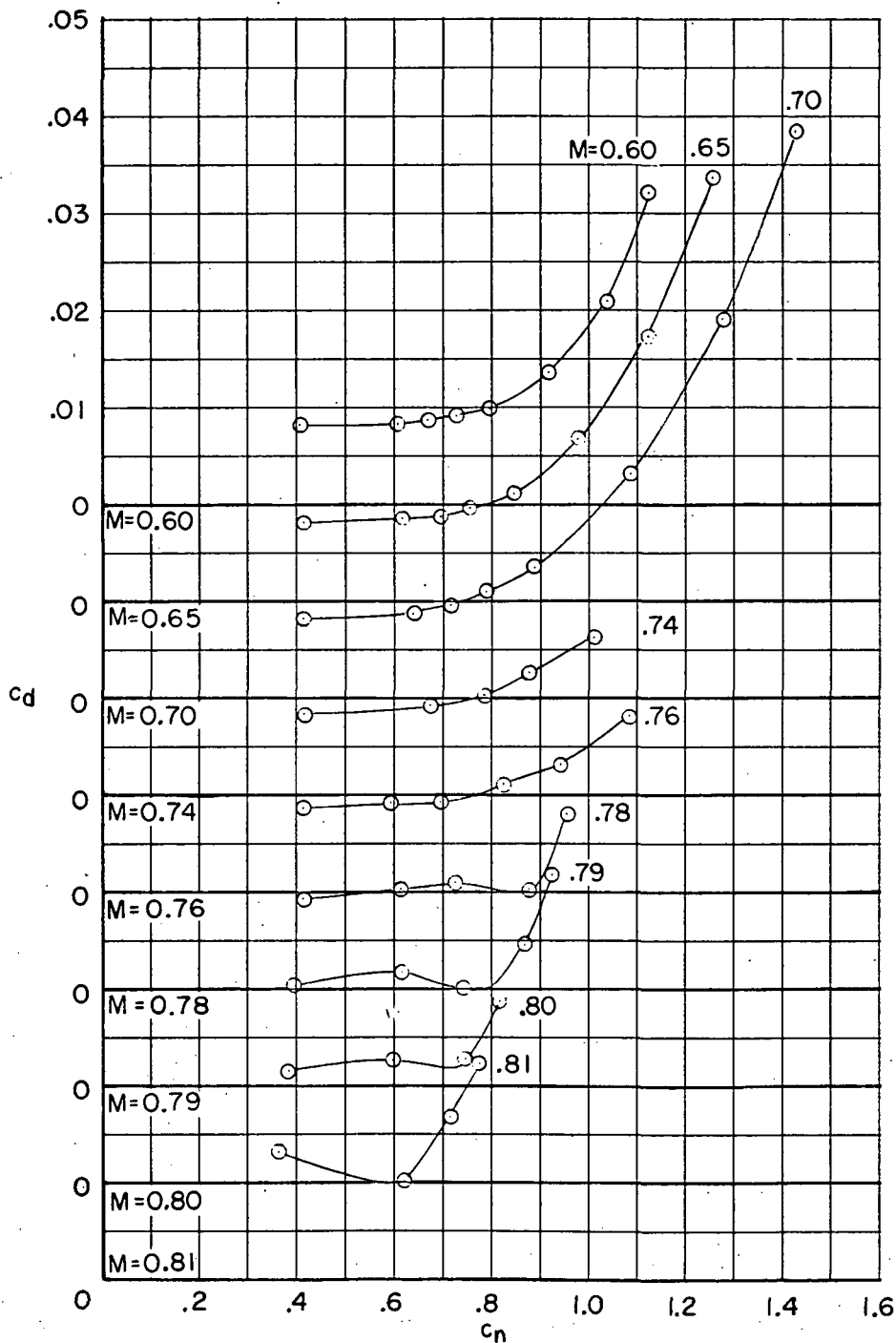


Figure 7.- Variation of section drag coefficient, angle of attack, and section pitching-moment coefficient at various Mach numbers for a 10-percent-thick supercritical airfoil with 1.0-percent-thick trailing edge with cavity (airfoil 9a). Data from reference 2.

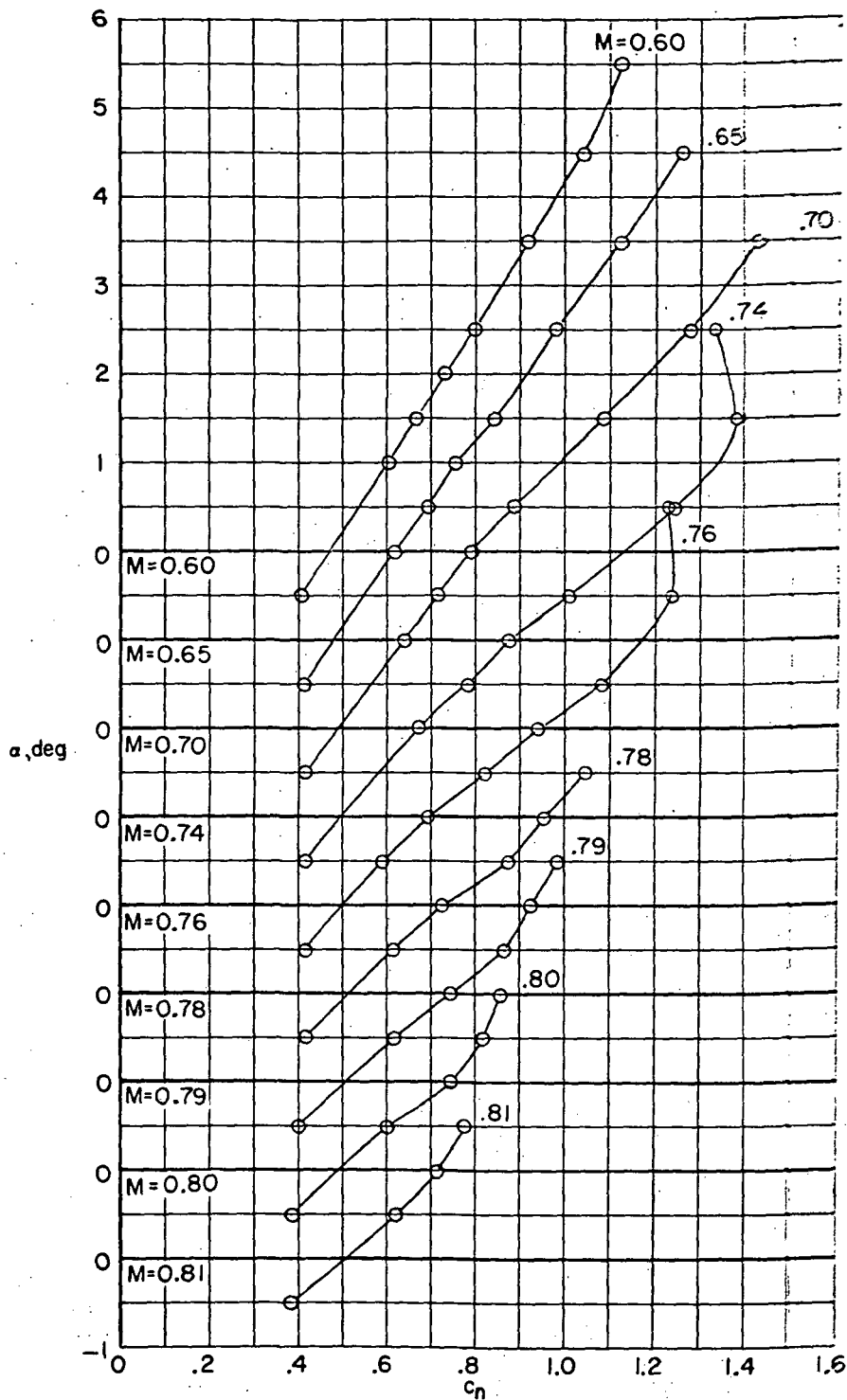


Figure 7.- Continued.

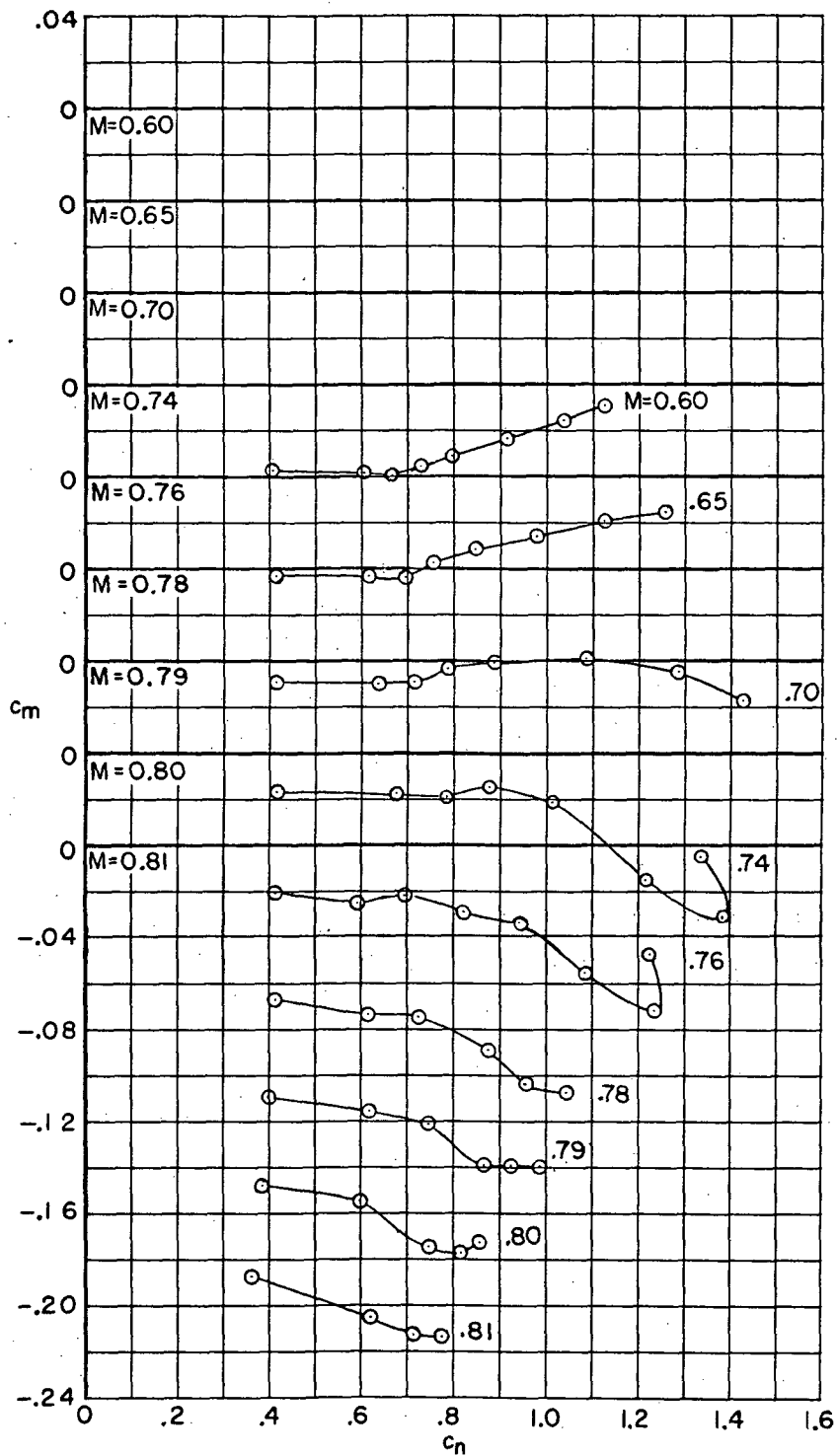
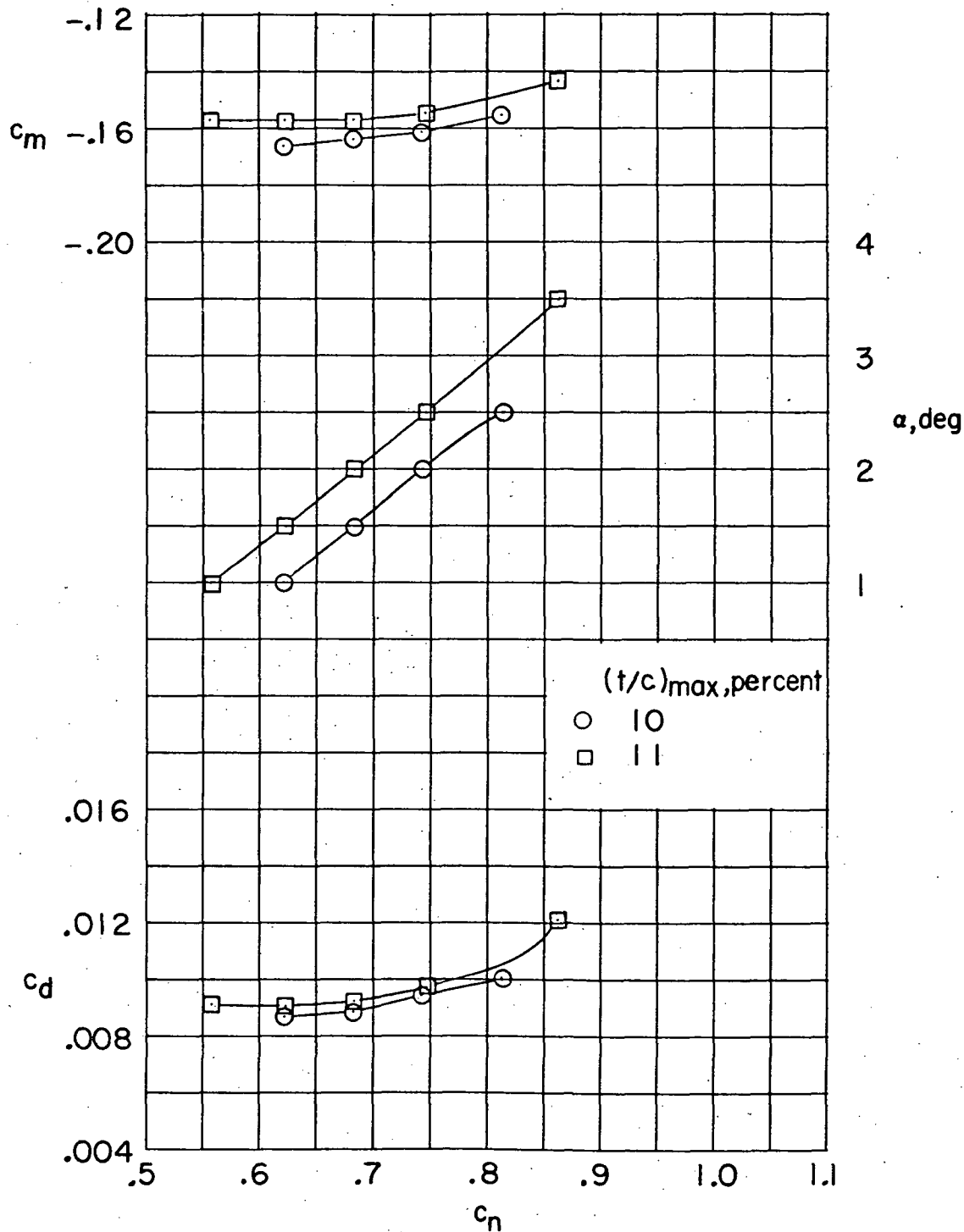
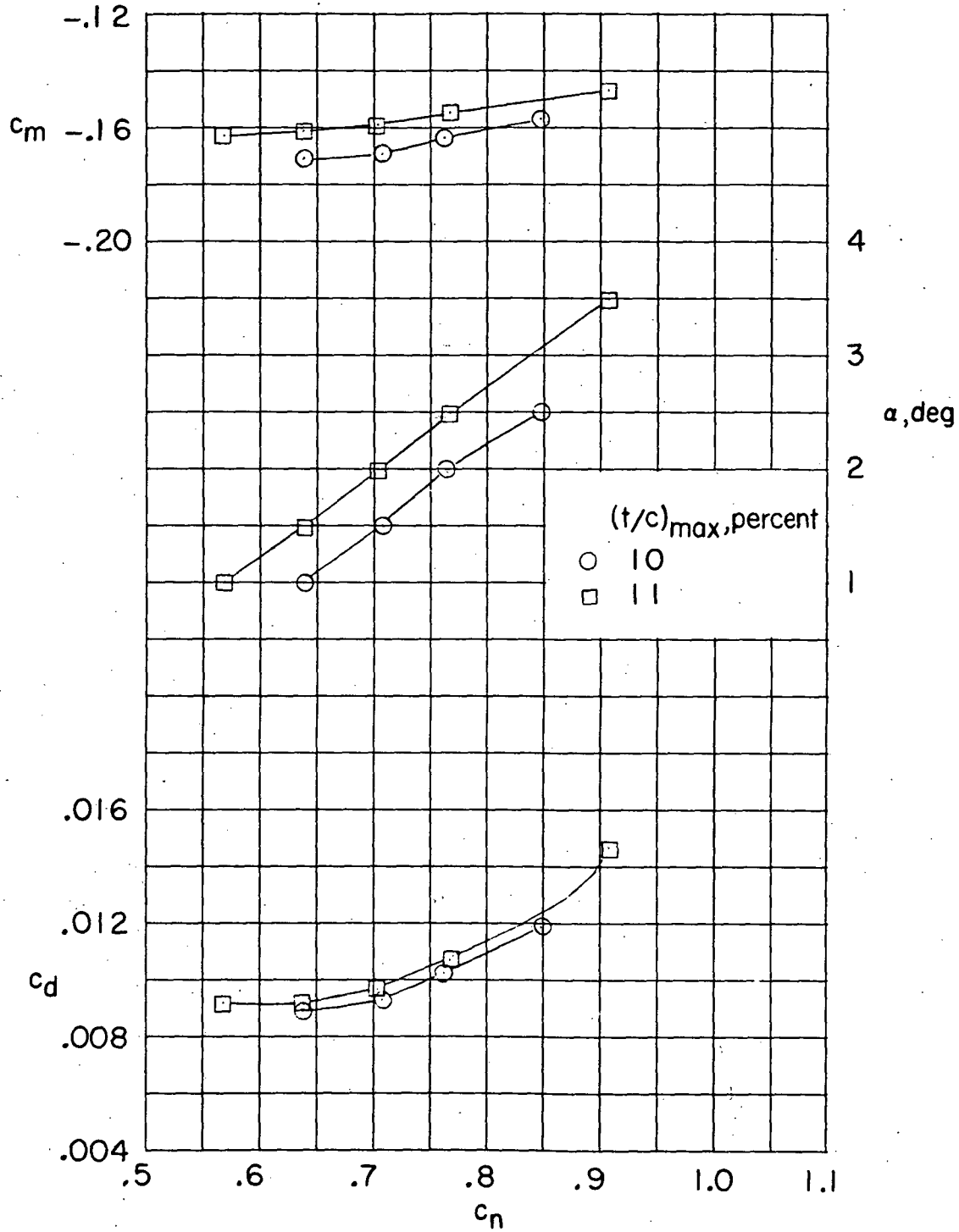


Figure 7.- Concluded.



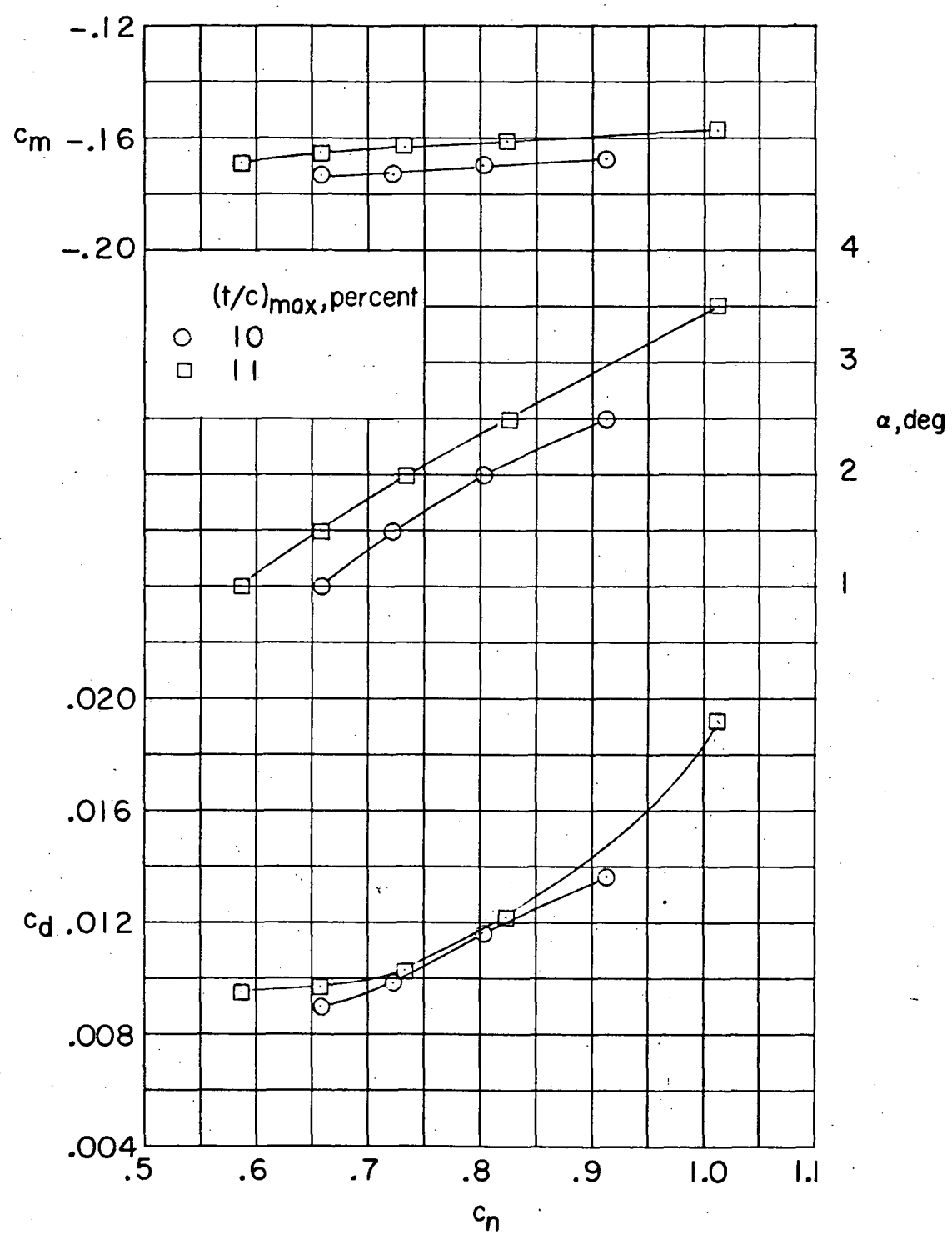
(a) $M = 0.60$.

Figure 8.- Comparison of supercritical airfoils with maximum thickness-chord ratios of 10 and 11 percent.



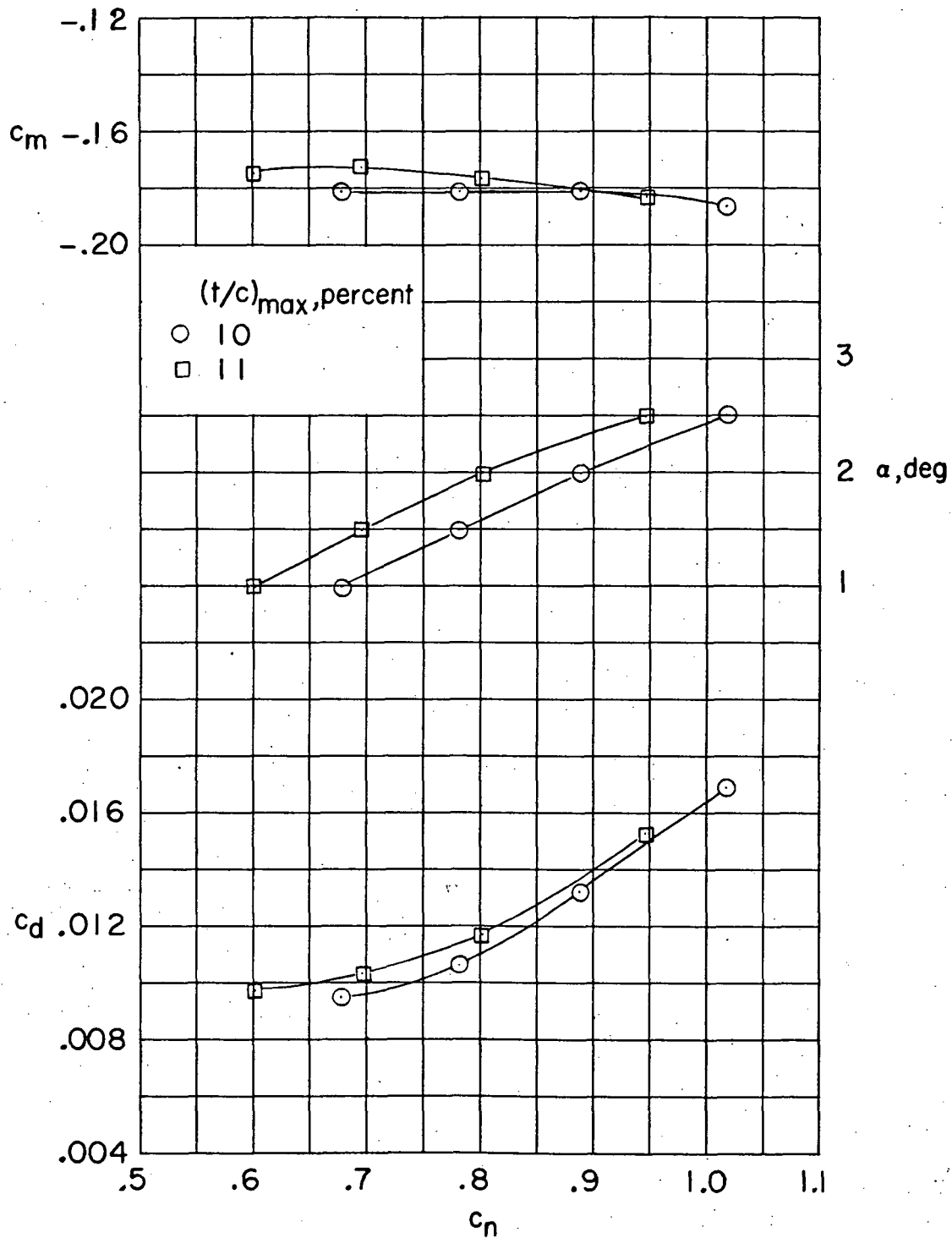
(b) $M = 0.65$.

Figure 8.- Continued.



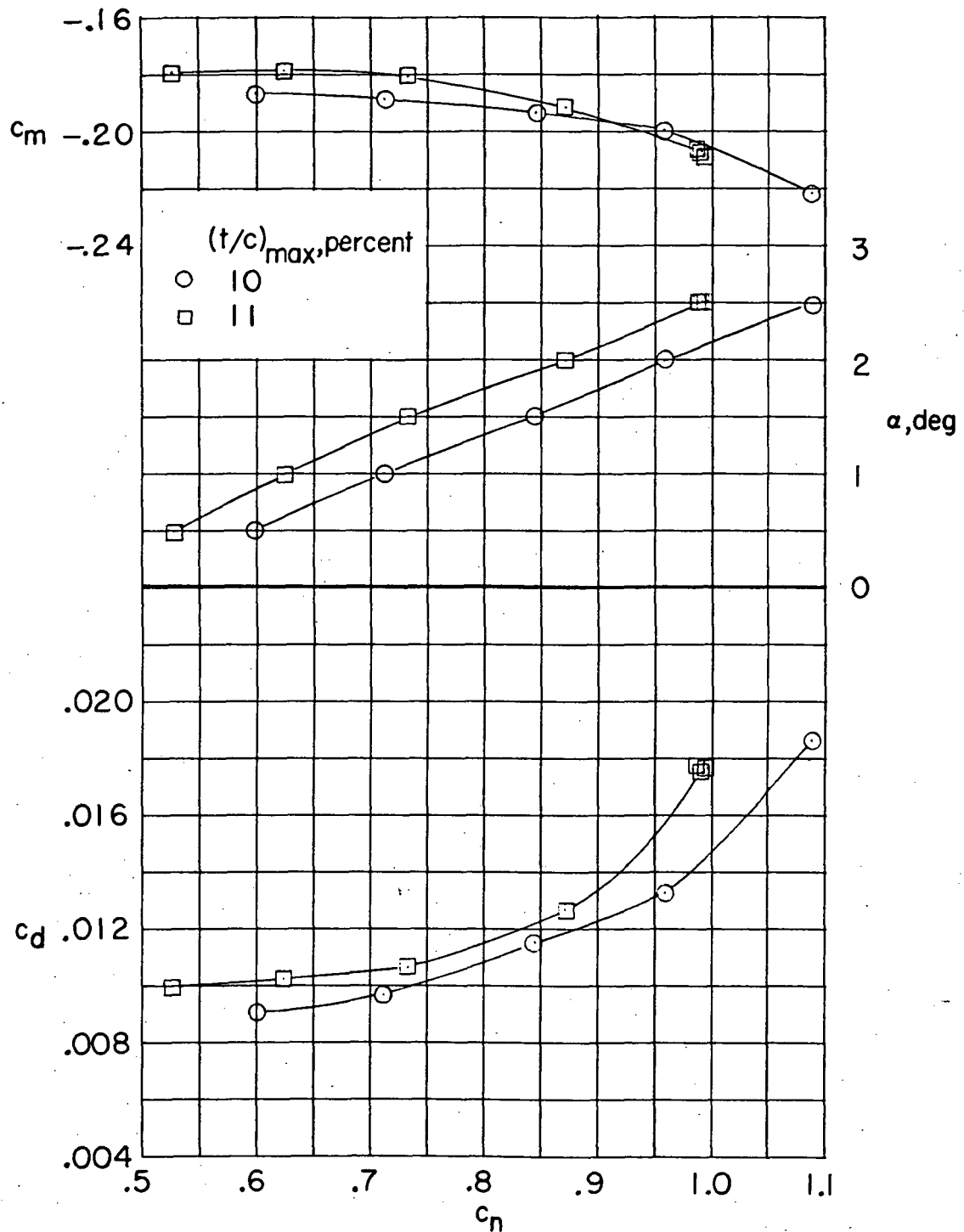
(c) $M = 0.70$.

Figure 8.- Continued.



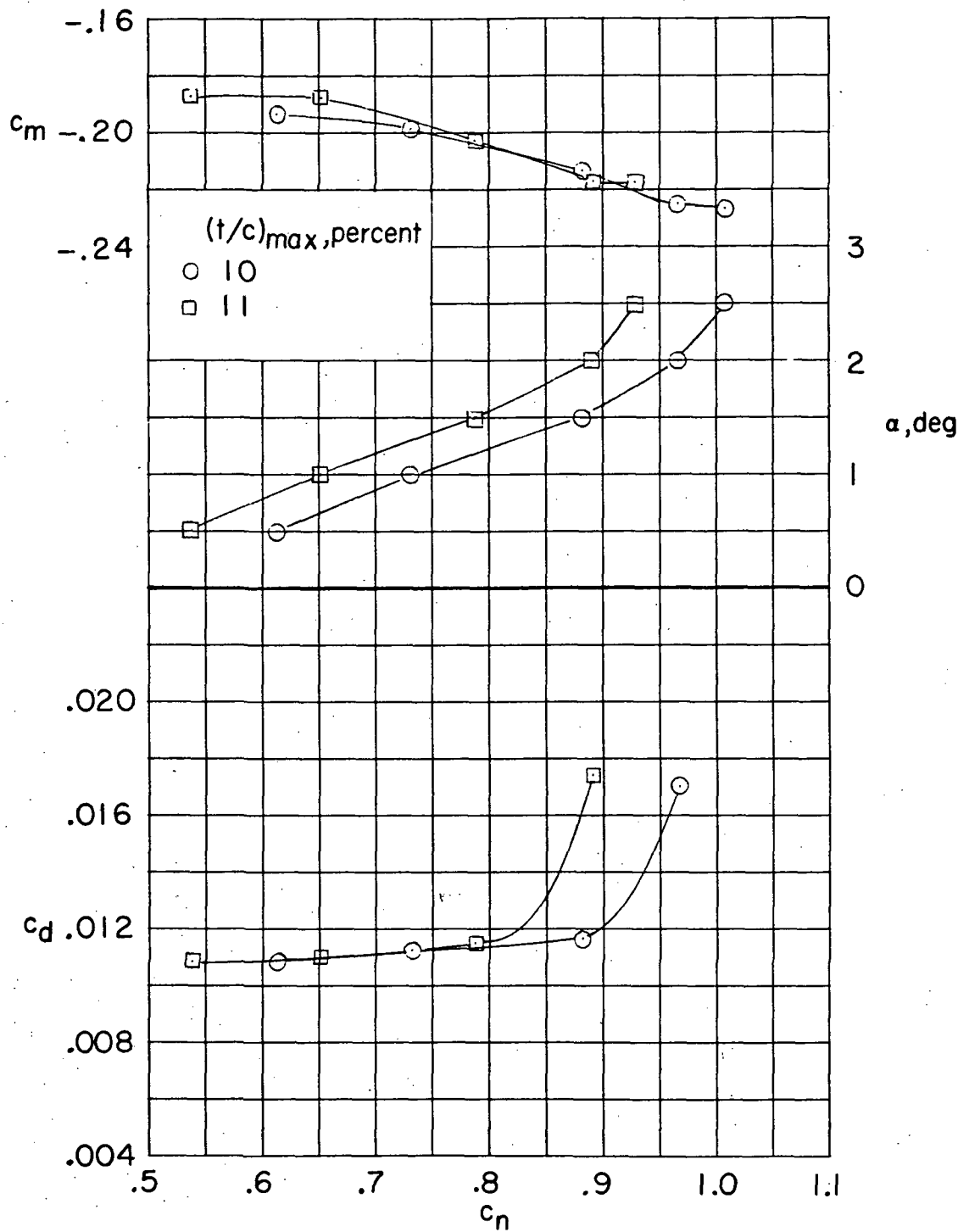
(d) $M = 0.74$.

Figure 8.- Continued.



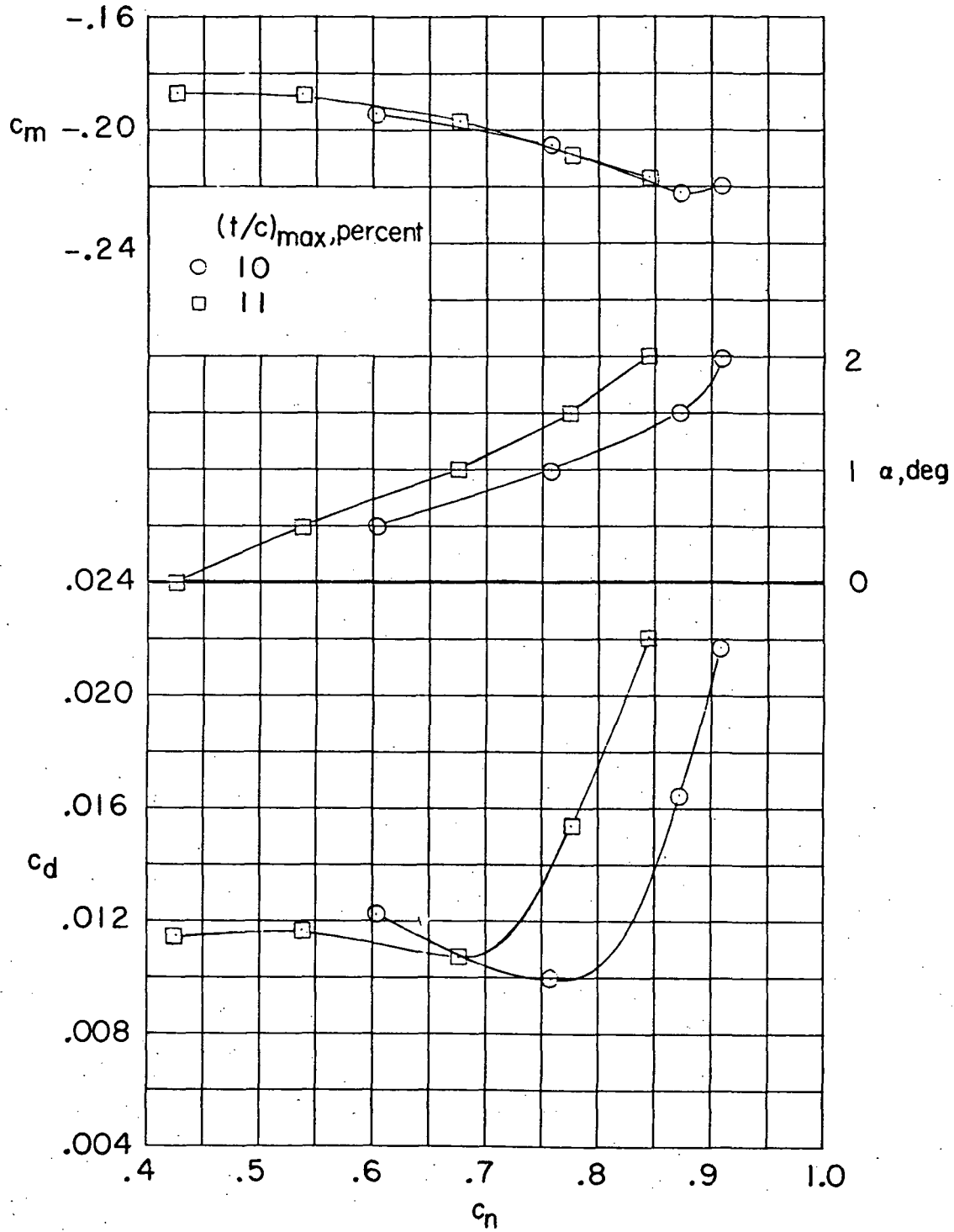
(e) $M = 0.76$.

Figure 8.- Continued.



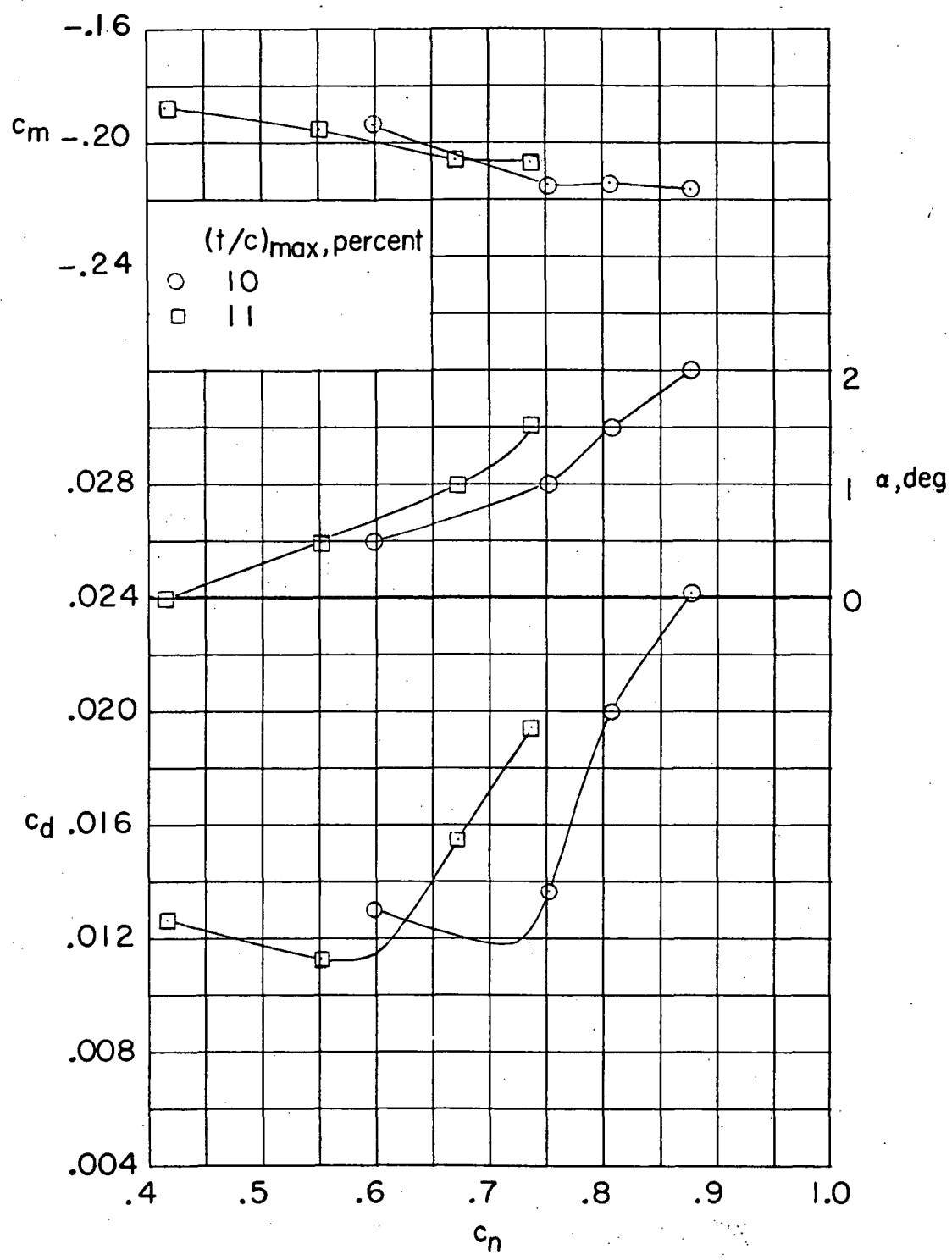
(f) $M = 0.78$.

Figure 8.- Continued.



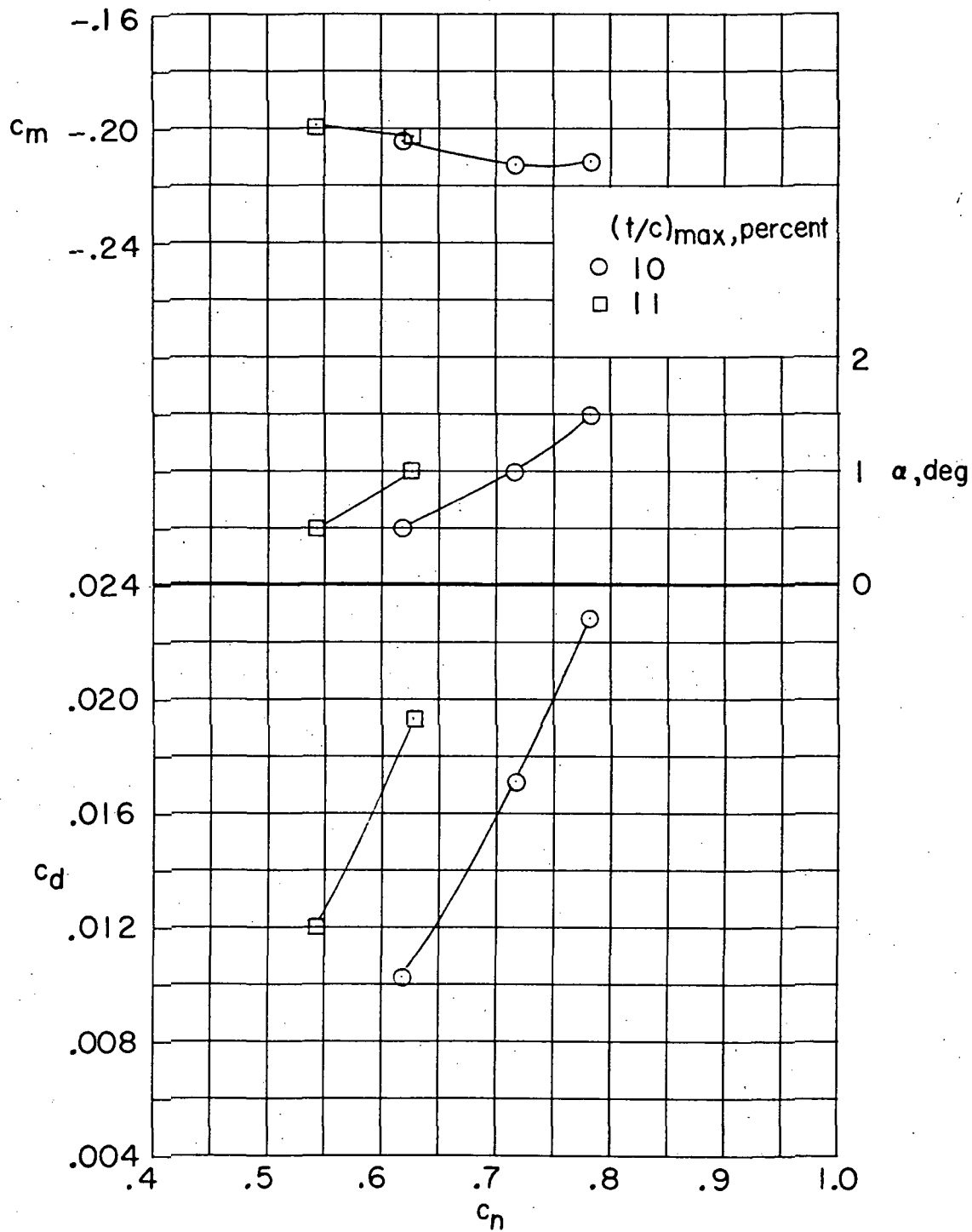
(g) $M = 0.79$.

Figure 8.- Continued.



(h) $M = 0.80$.

Figure 8.- Continued.



(i) $M = 0.81$.

Figure 8.- Concluded.

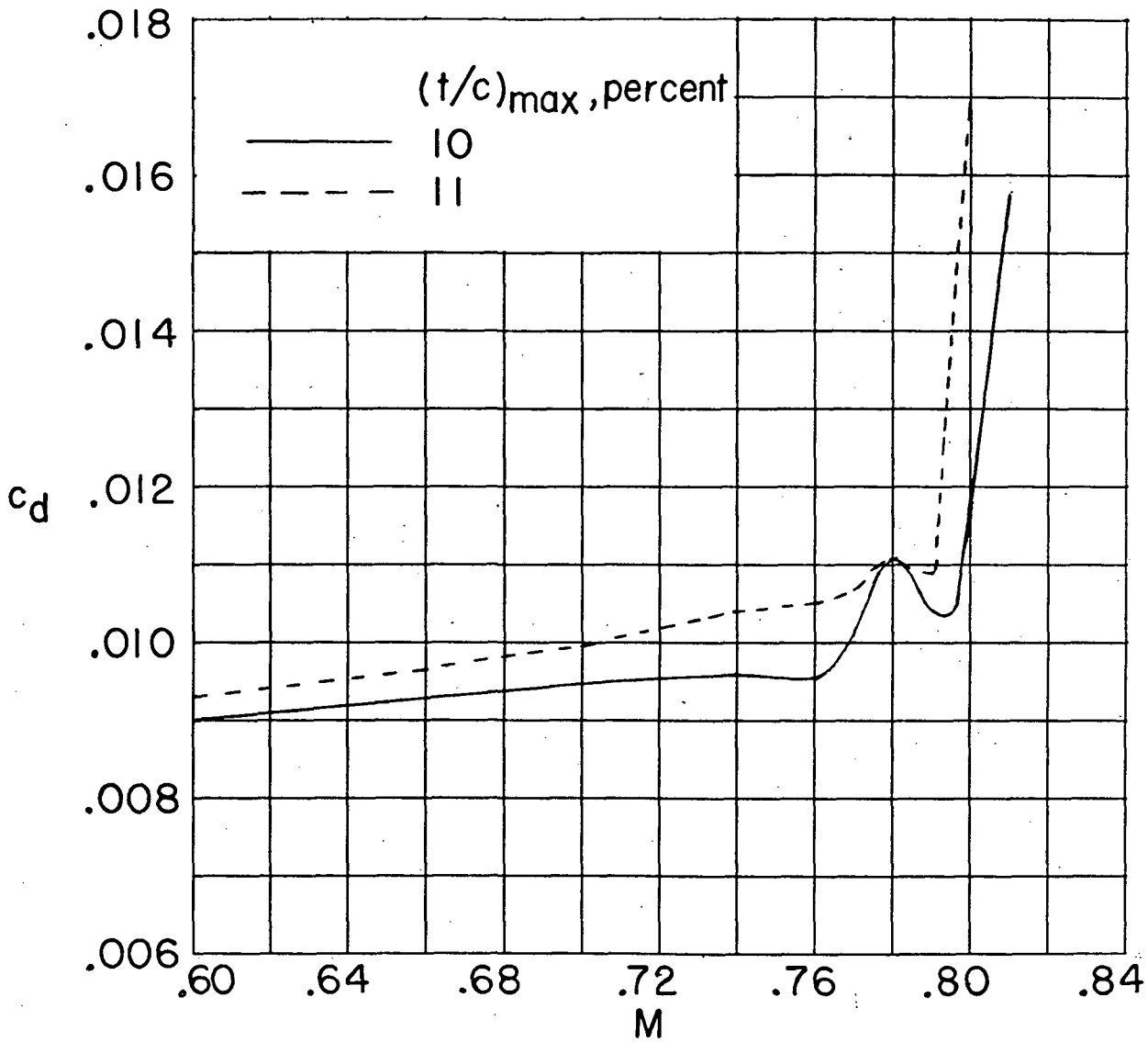
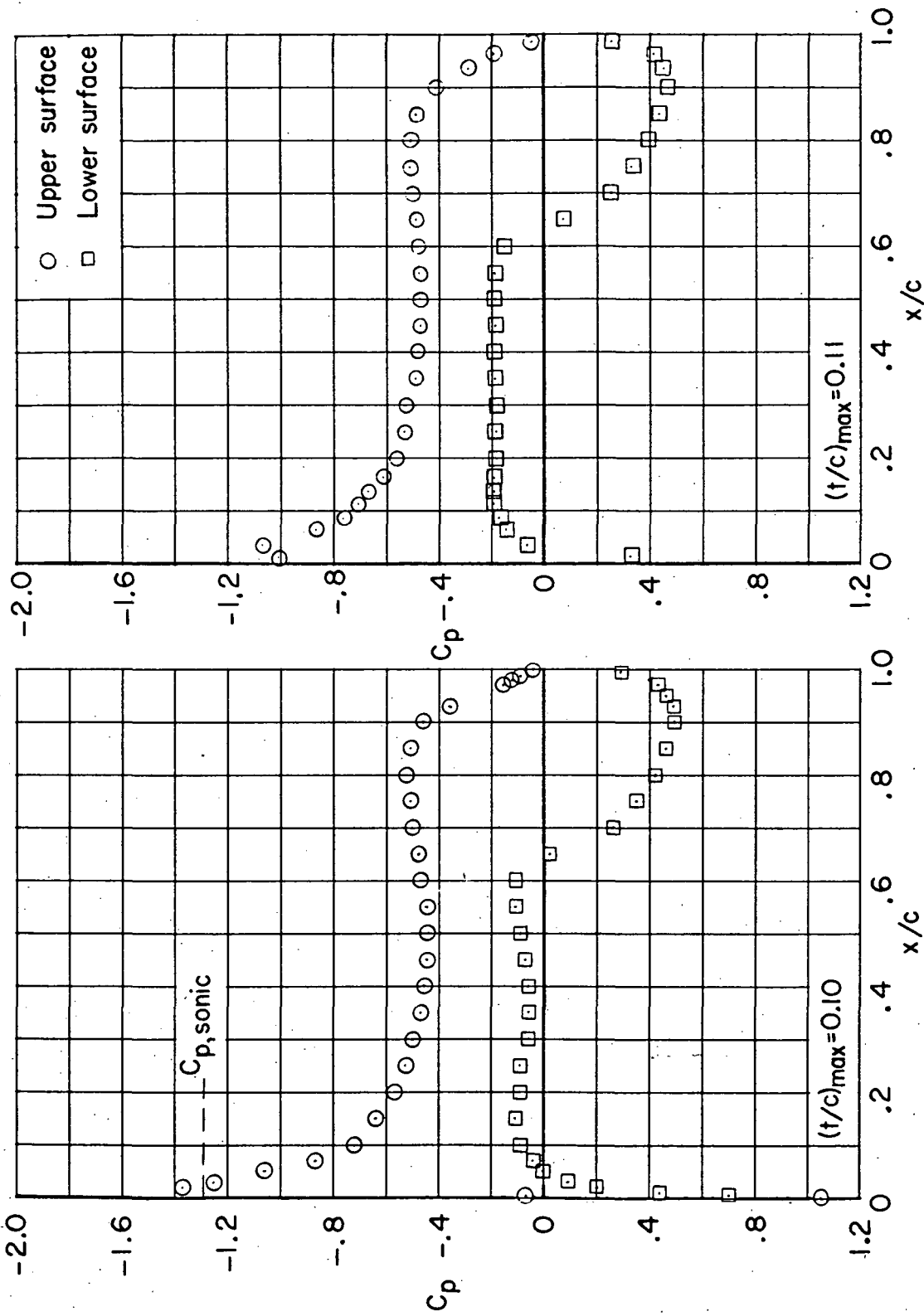
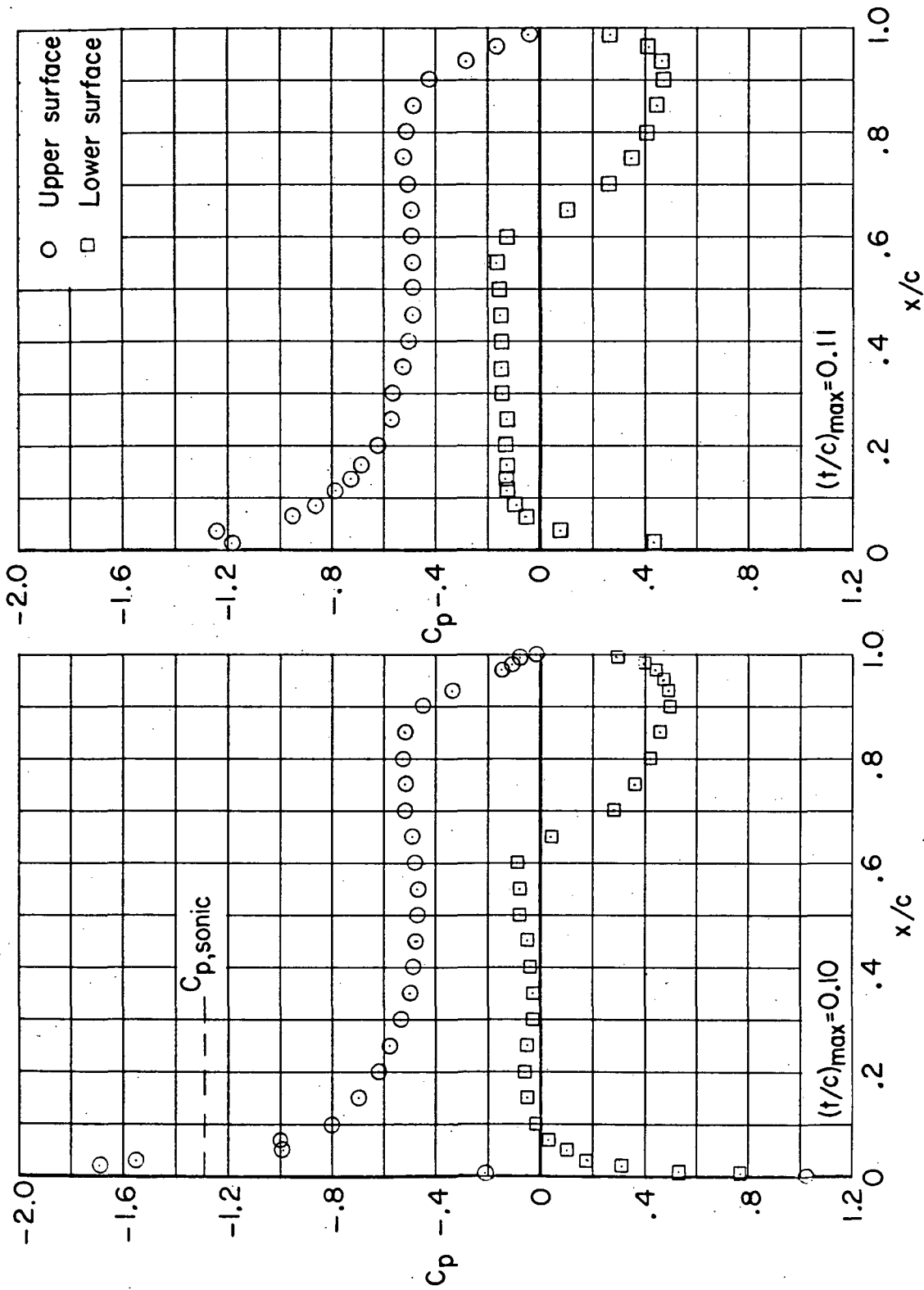


Figure 9.- Comparison of variation of section drag coefficient with Mach number at section normal-force coefficient of 0.7 for supercritical airfoils with maximum thickness-chord ratios of 10 and 11 percent.



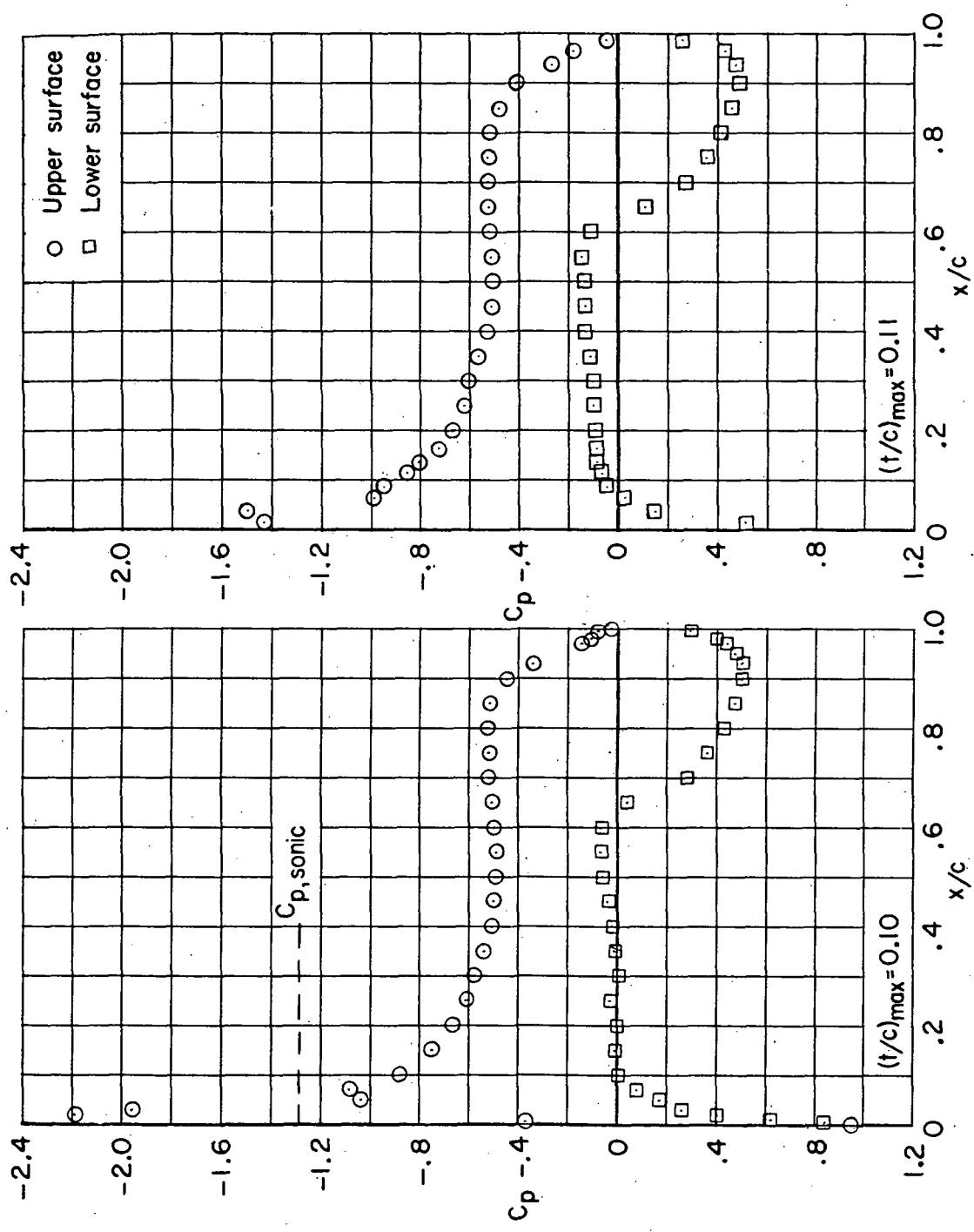
(a) $M = 0.60$; $\alpha = 1.00^\circ$.

Figure 10.- Chordwise pressure distributions for supercritical airfoils with maximum thickness-chord ratios of 10 and 11 percent.



(b) $M = 0.60$; $\alpha = 1.50^\circ$.

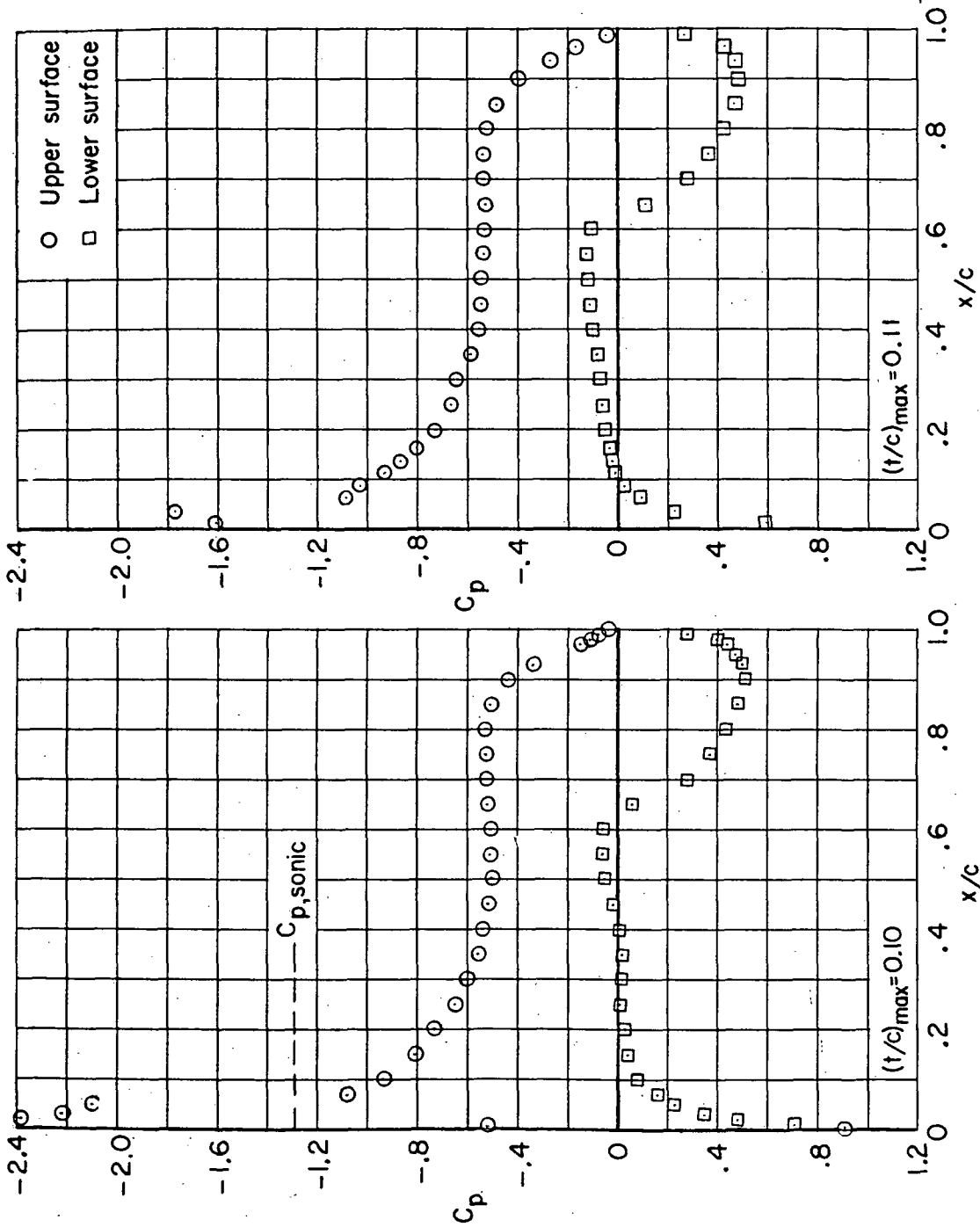
Figure 10.- Continued.



(c) $M = 0.60$; $\alpha = 2.0^\circ$.

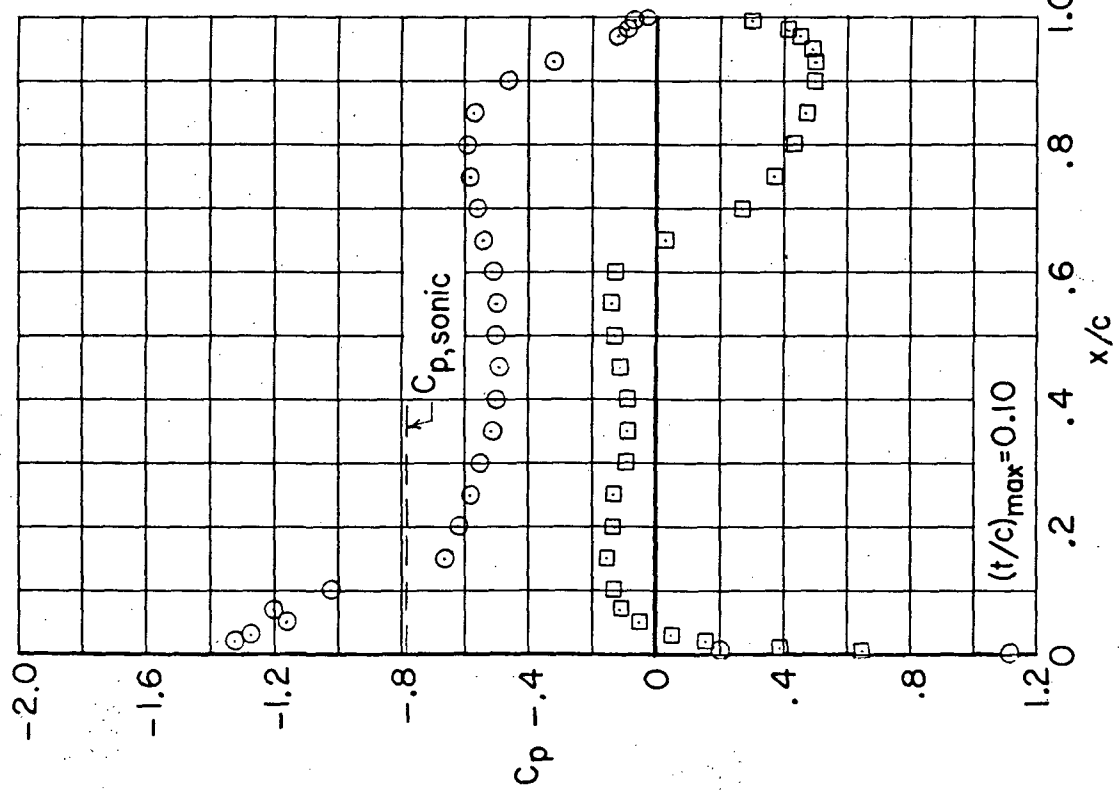
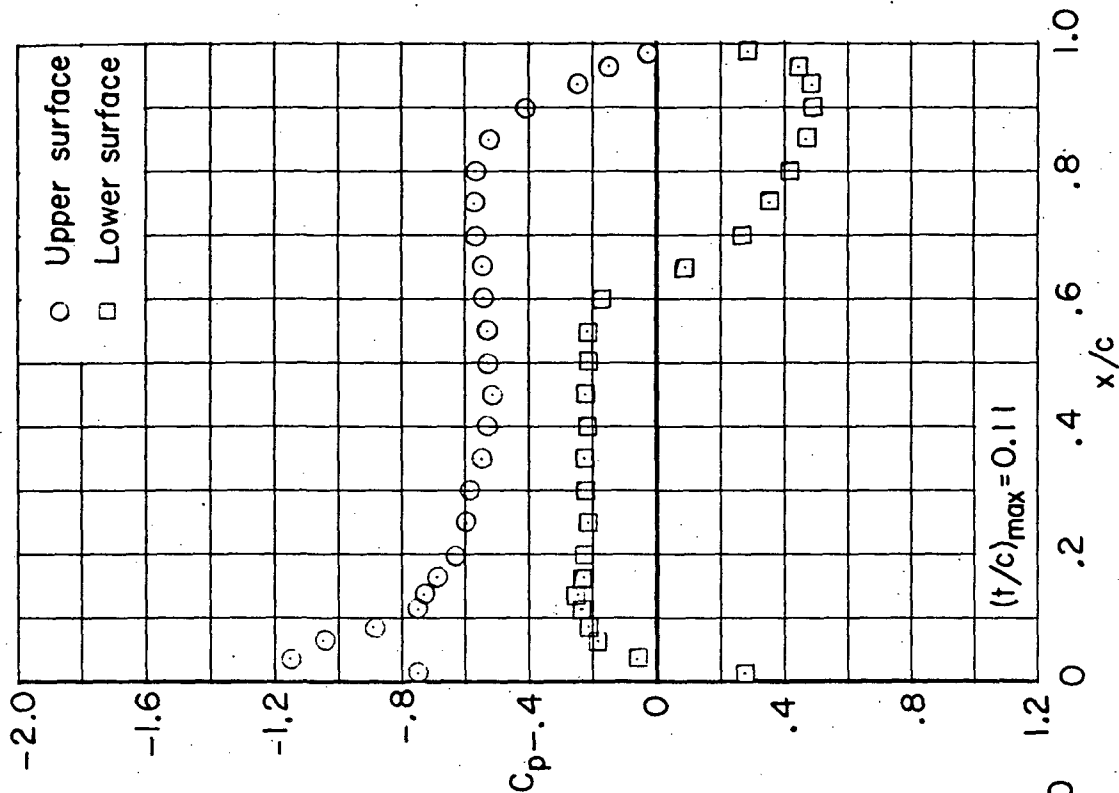
Figure 10.- Continued.

ORIGINAL PAGE IS
OF POOR QUALITY



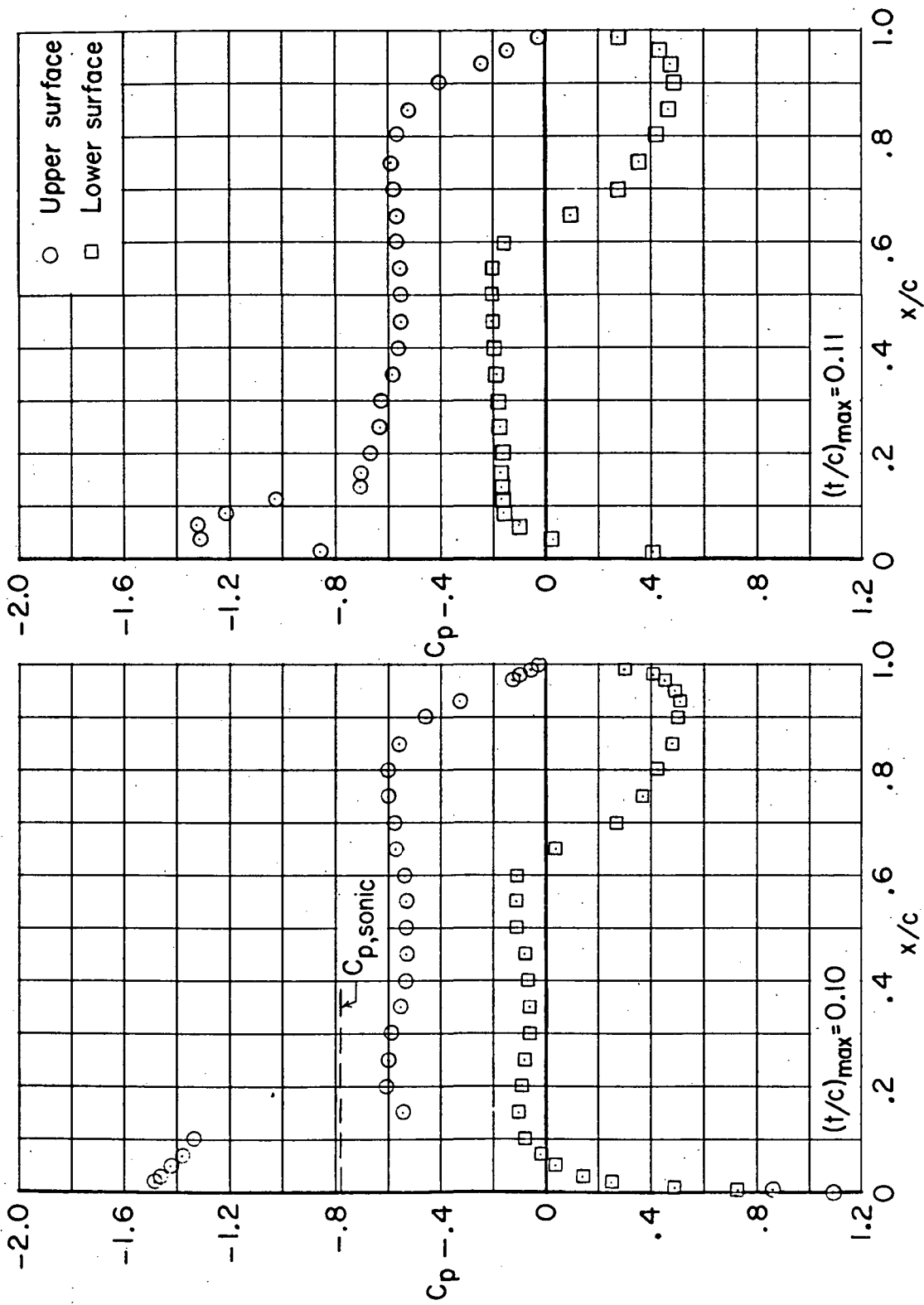
(d) $M = 0.60$; $\alpha = 2.50^\circ$.

Figure 10.- Continued.



(e) $M = 0.70$; $\alpha = 1.0^\circ$.

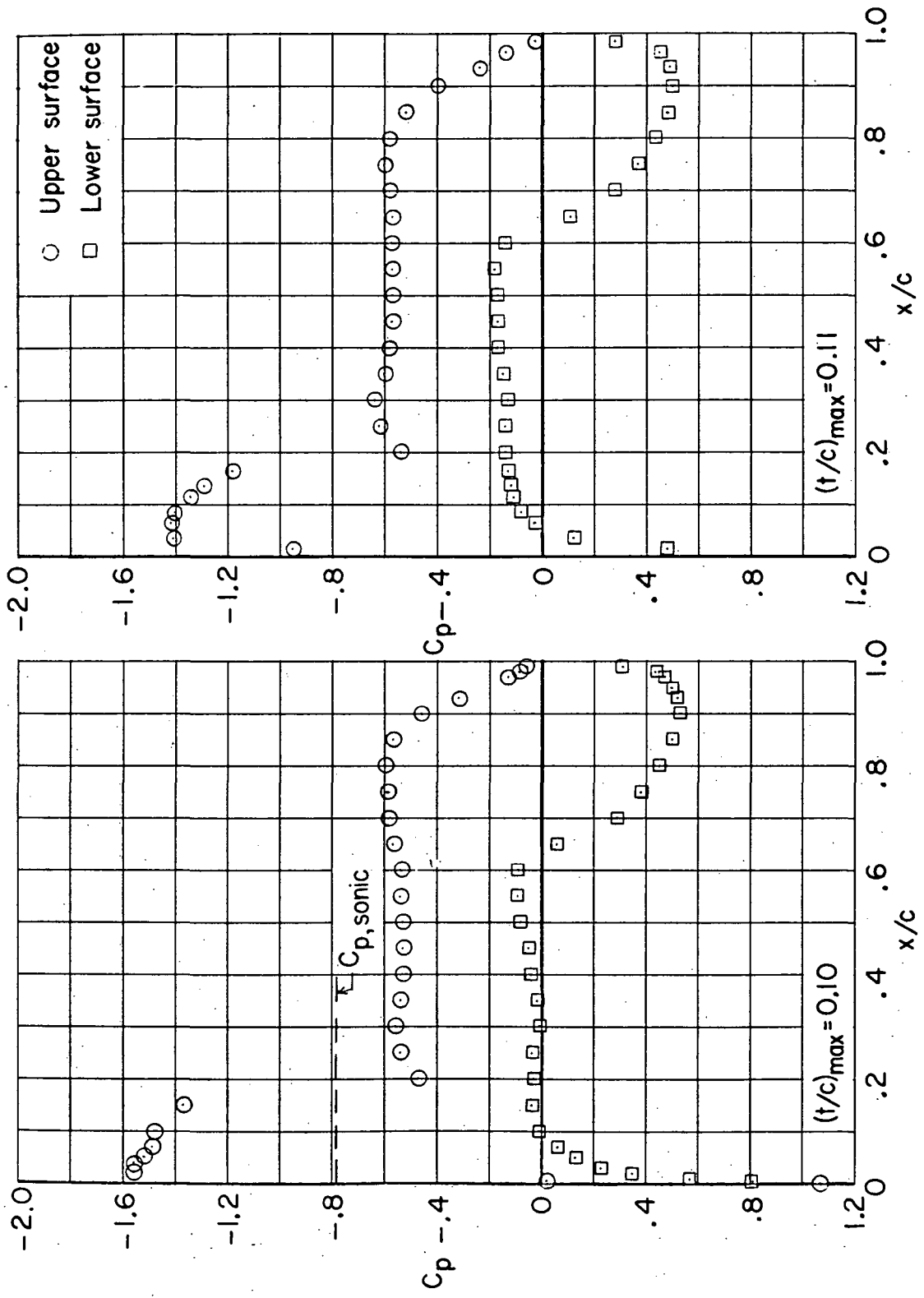
Figure 10.- Continued.



(f) $M = 0.70$; $\alpha = 1.5^\circ$.

Figure 10.- Continued.

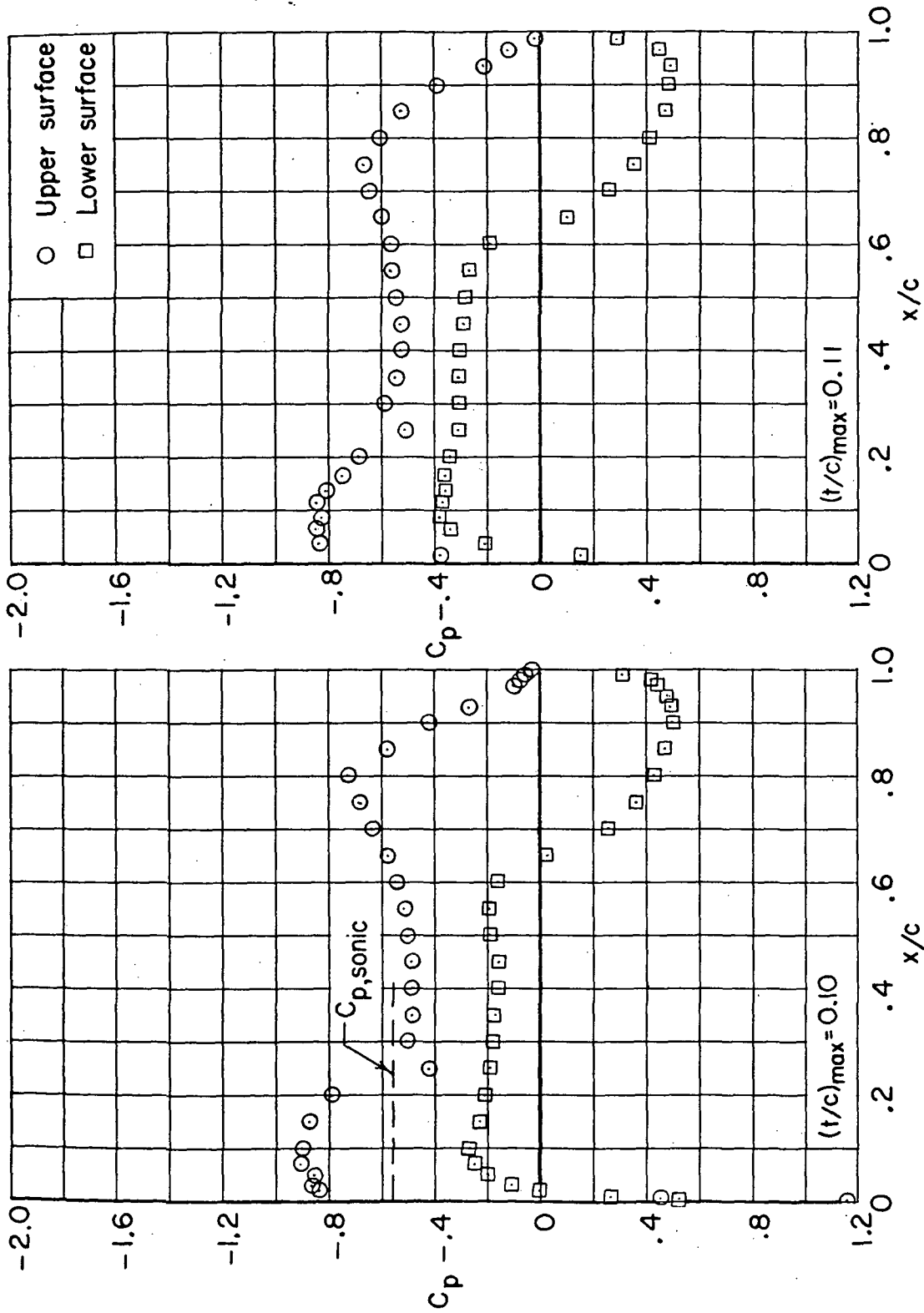
~~CONFIDENTIAL~~



(g) $M = 0.70$; $\alpha = 2.0^\circ$.

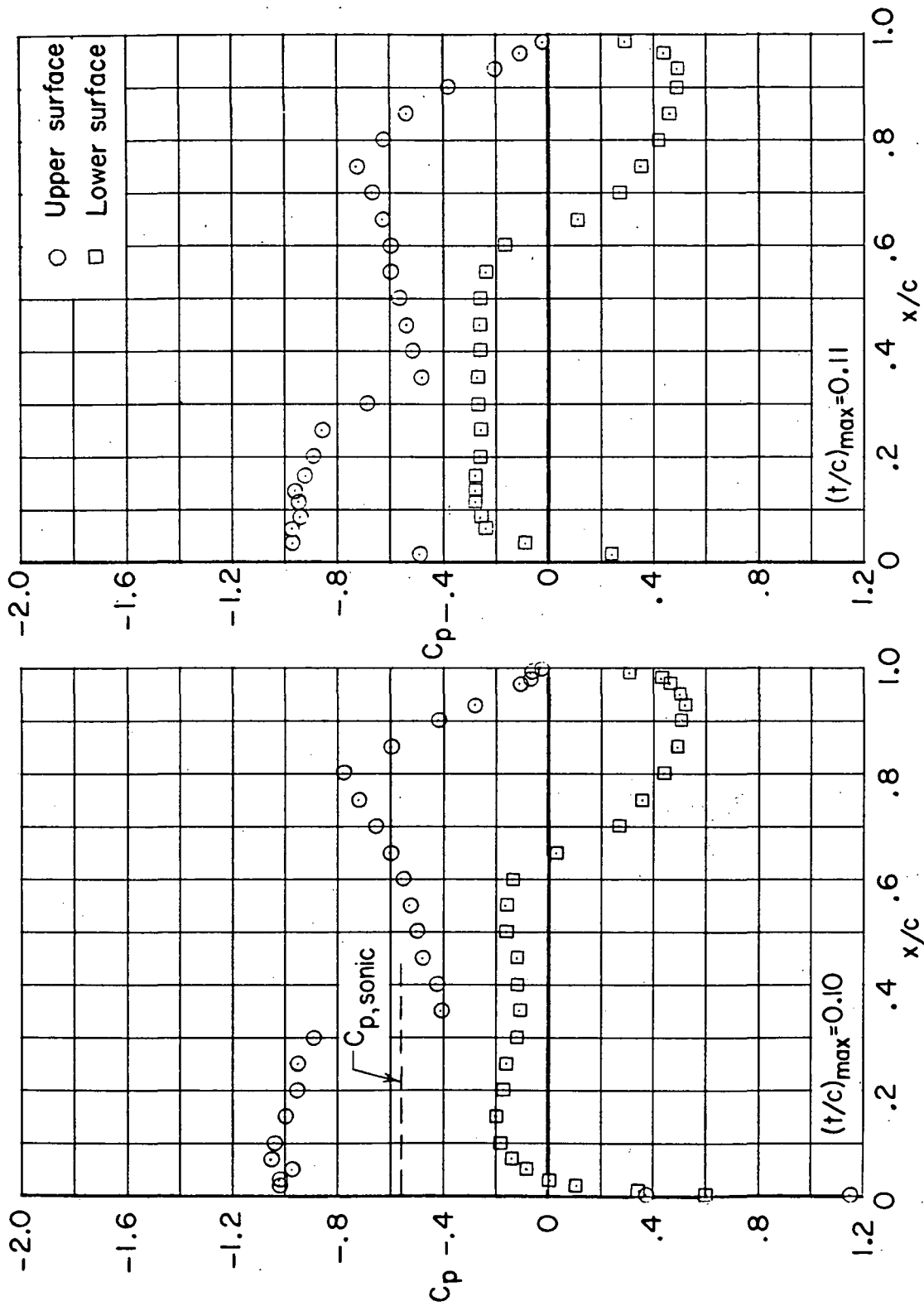
Figure 10.- Continued.

~~CONFIDENTIAL~~



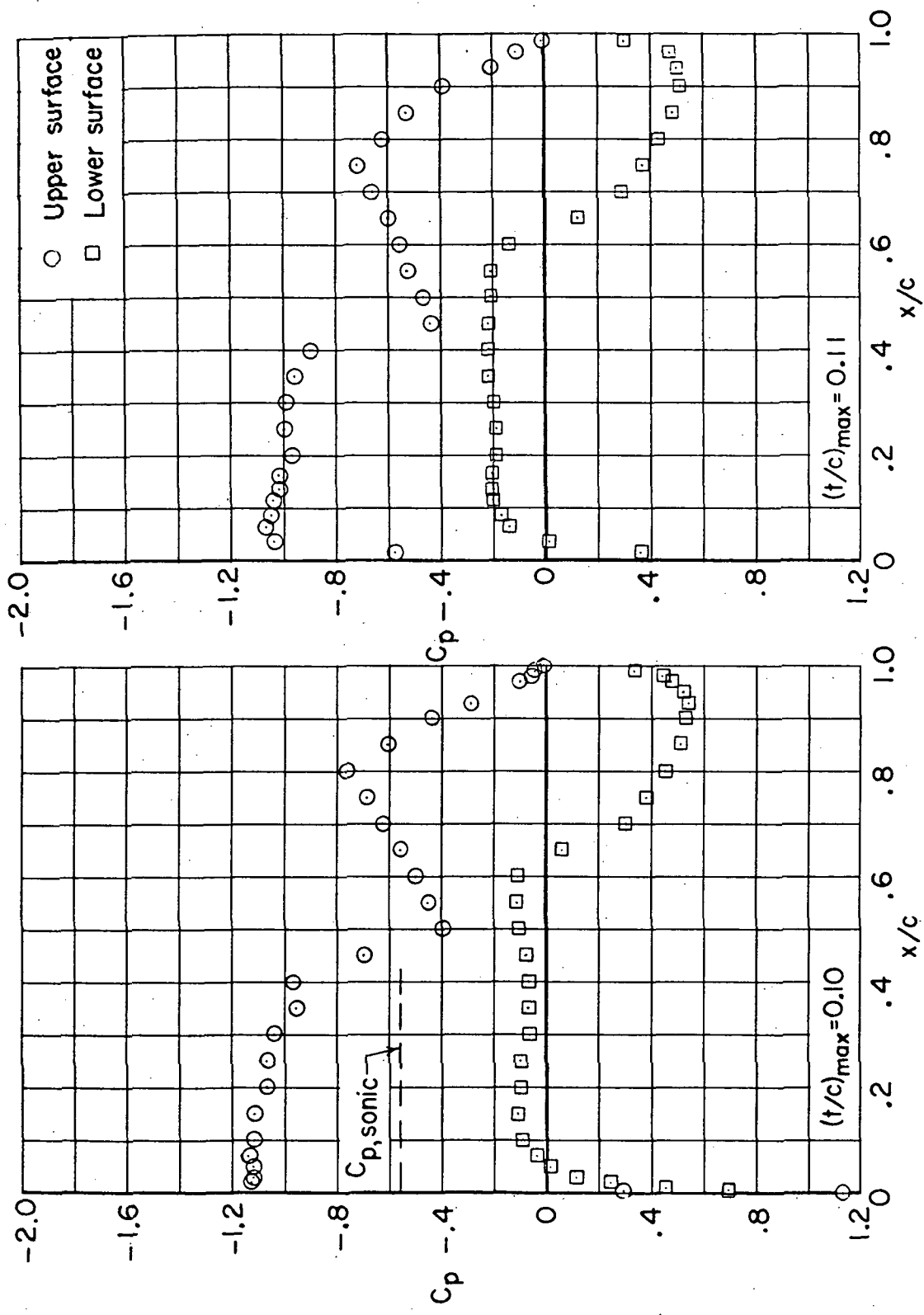
(h) $M = 0.76$; $\alpha = 0.5^\circ$.

Figure 10.- Continued.



(i) $M = 0.76$; $\alpha = 1.0^\circ$.

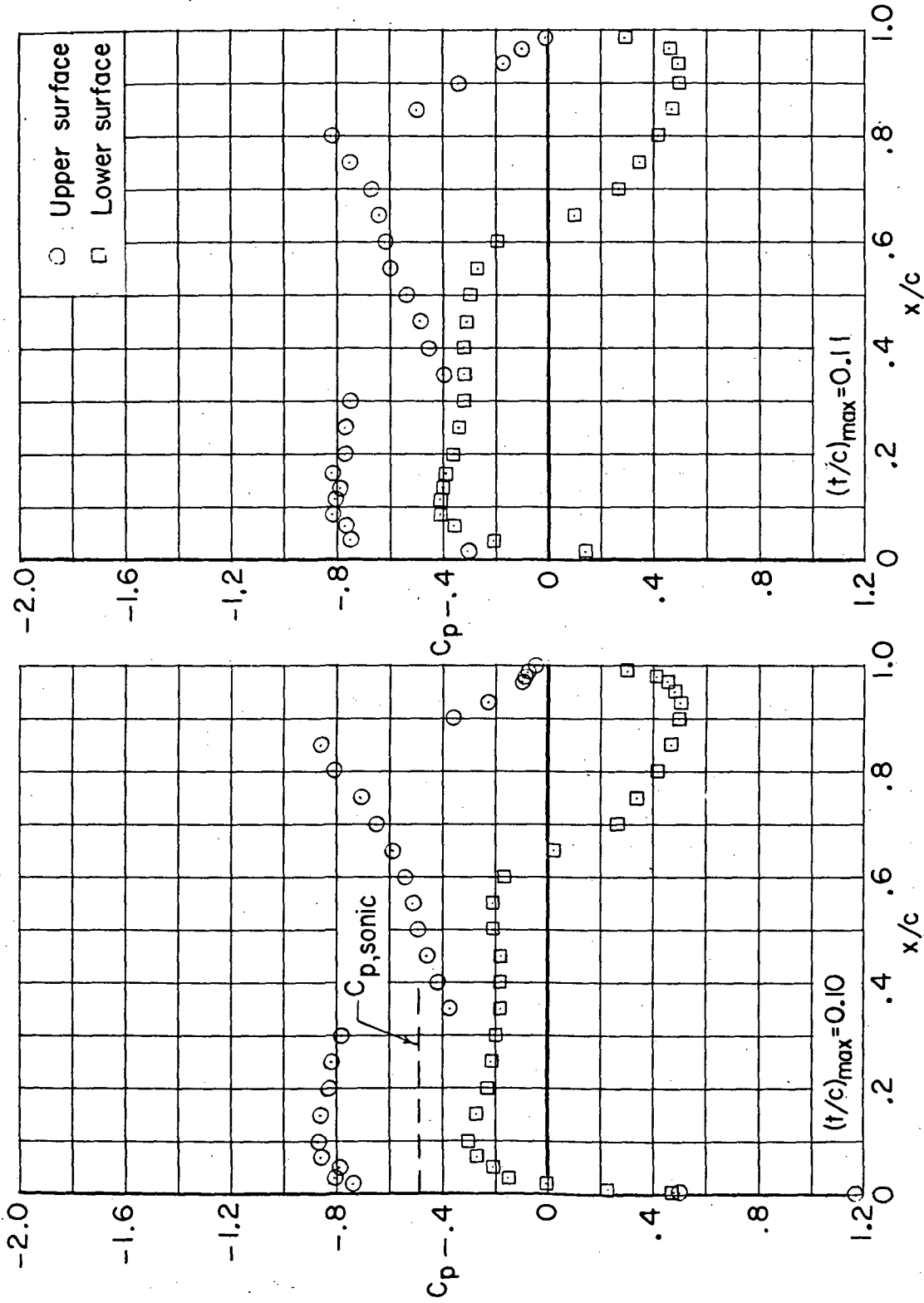
Figure 10.- Continued.



(j) $M = 0.76$; $\alpha = 1.50$.

Figure 10.- Continued.

~~CONFIDENTIAL~~



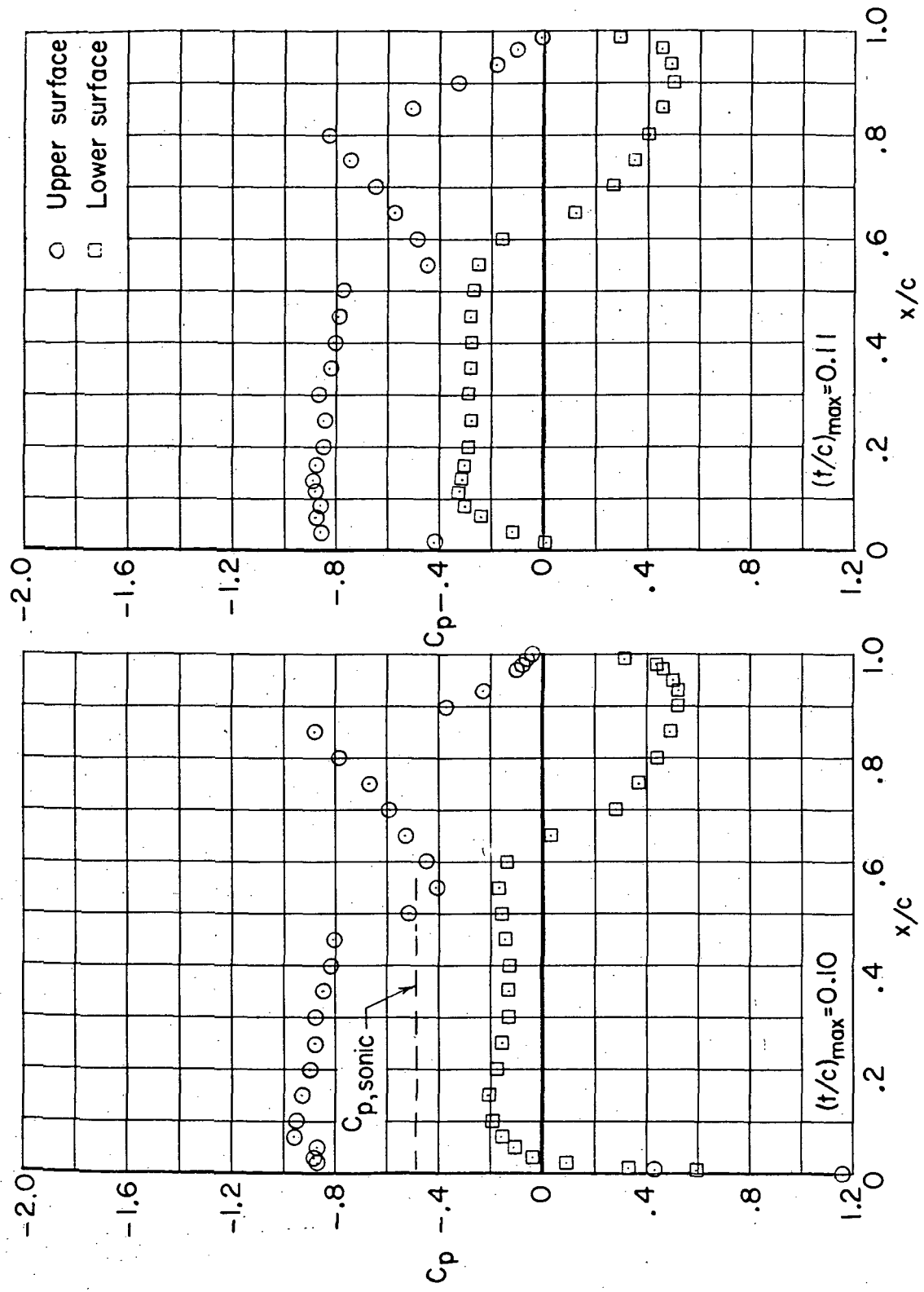
(k) $M = 0.78$; $\alpha = 0.5^\circ$.

Figure 10.- Continued.

~~CONFIDENTIAL~~

~~CONFIDENTIAL~~

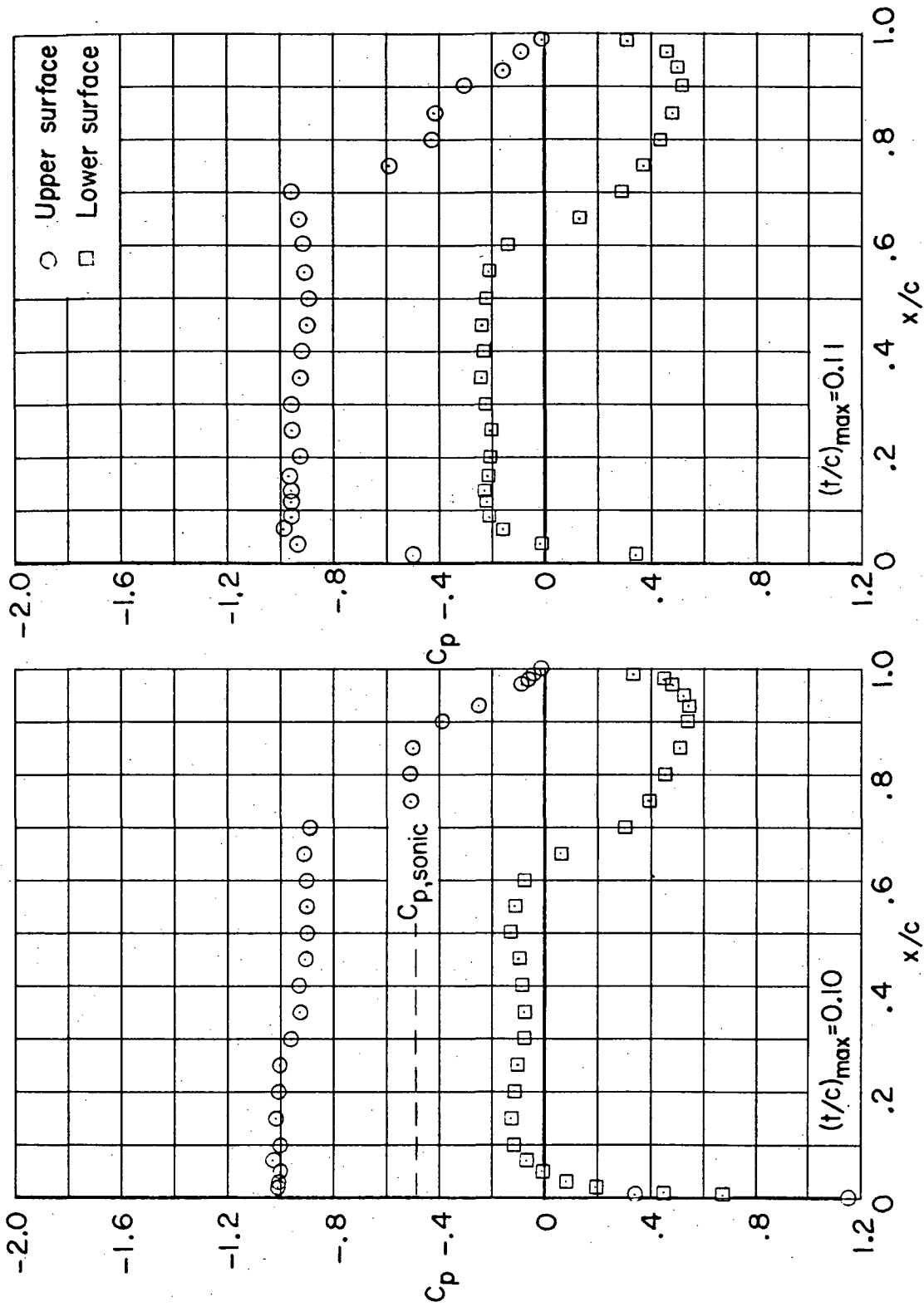
ORIGINAL PAGE IS
OF POOR QUALITY



(1) $M = 0.78$; $\alpha = 1.0^\circ$.

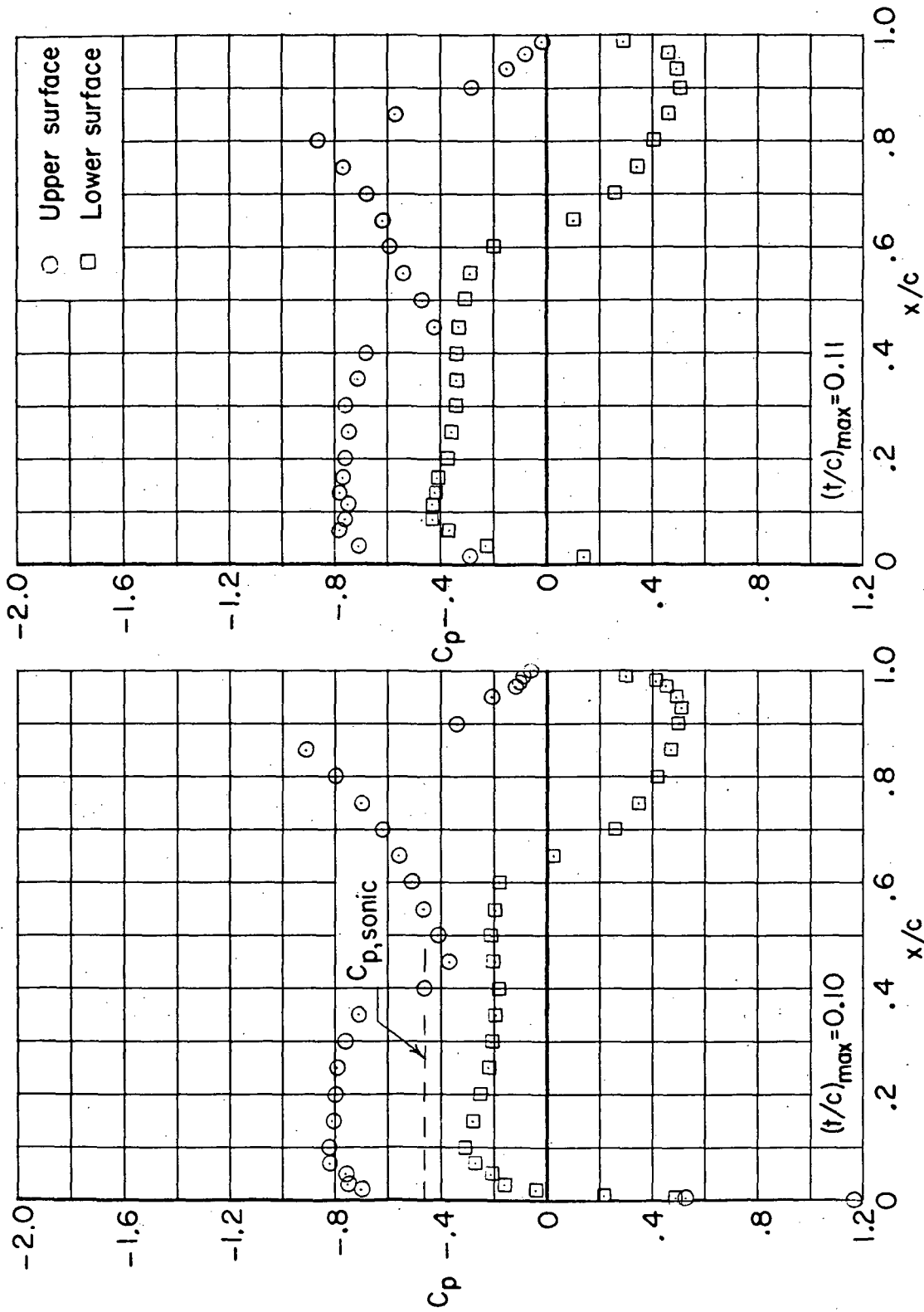
Figure 10.- Continued.

~~CONFIDENTIAL~~



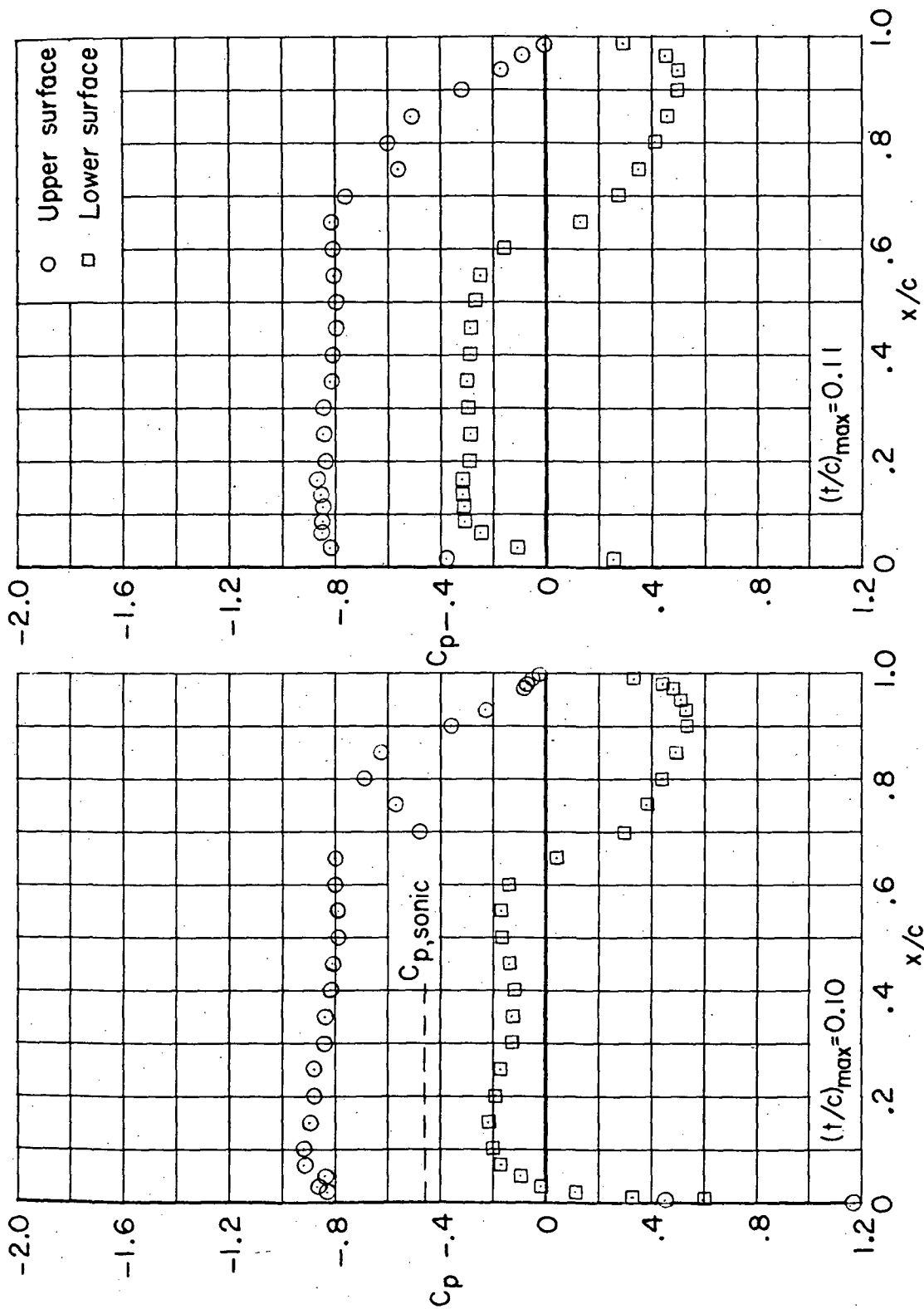
(m) $M = 0.78$; $\alpha = 1.50^\circ$.

Figure 10.- Continued.



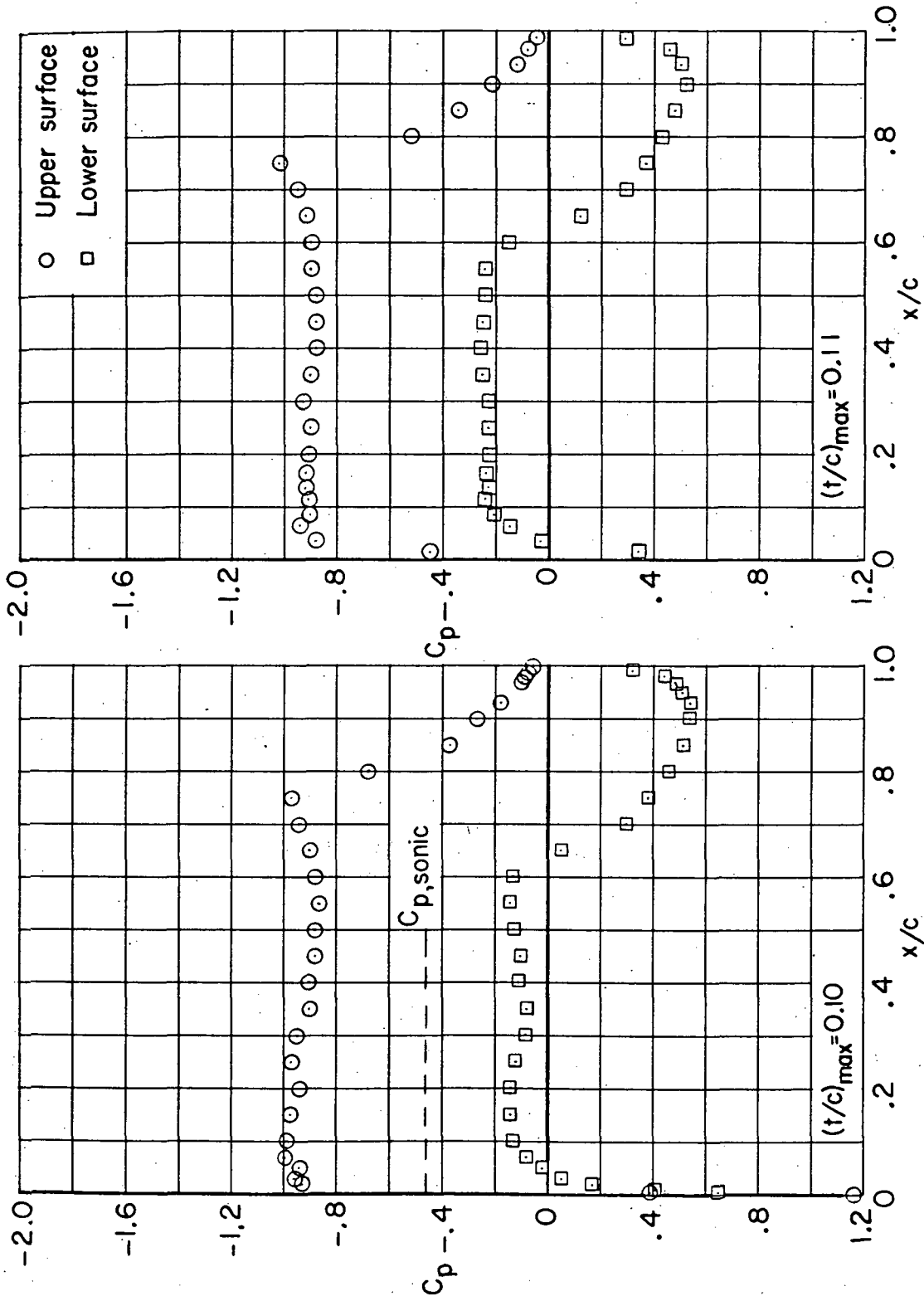
(n) $M = 0.79$; $\alpha = 0.5^\circ$.

Figure 10.- Continued.



(o) $M = 0.79$; $\alpha = 1.0^\circ$.

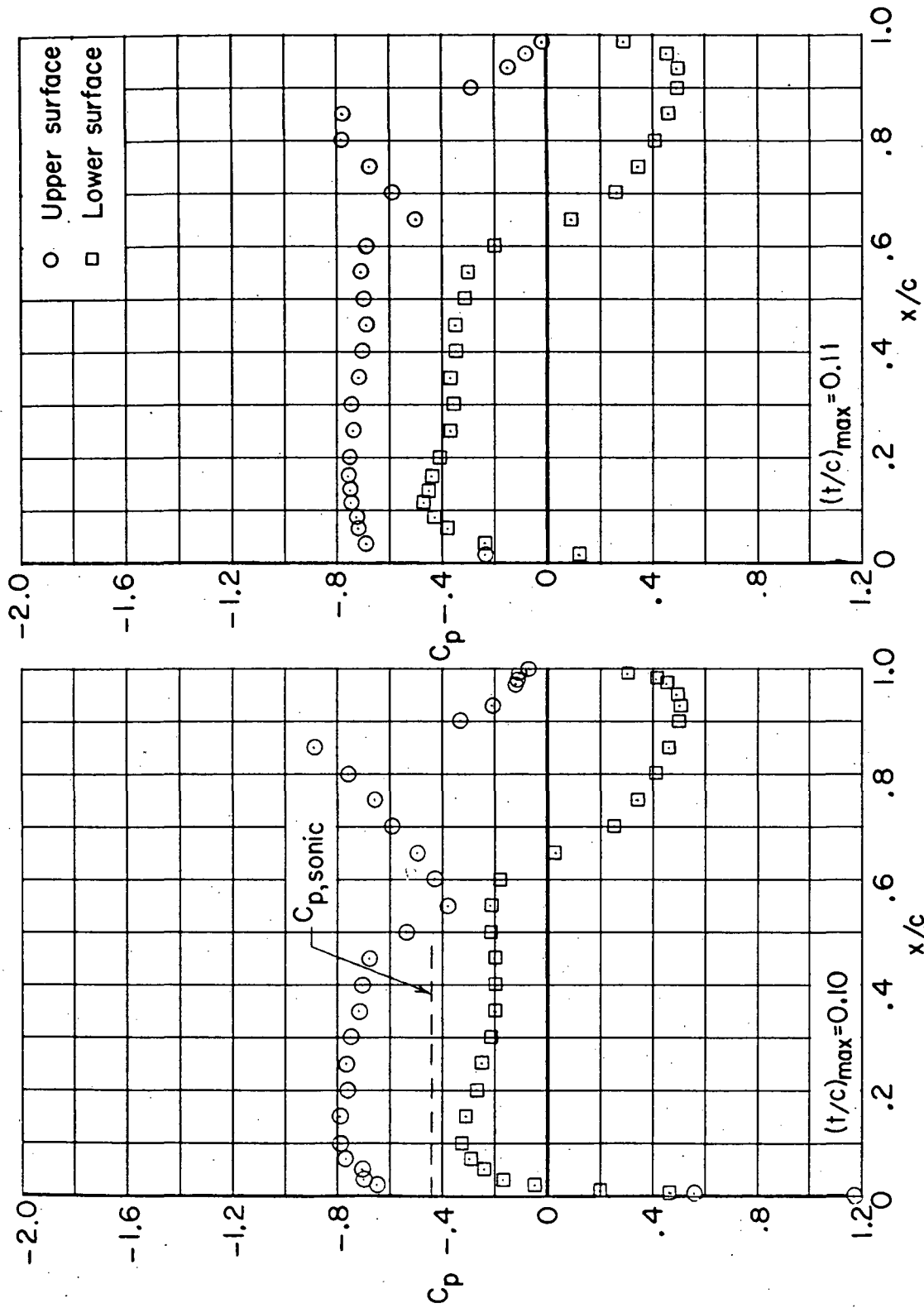
Figure 10.- Continued.



(p) $M = 0.79$; $\alpha = 1.50^\circ$.

Figure 10.- Continued.

~~CONFIDENTIAL~~

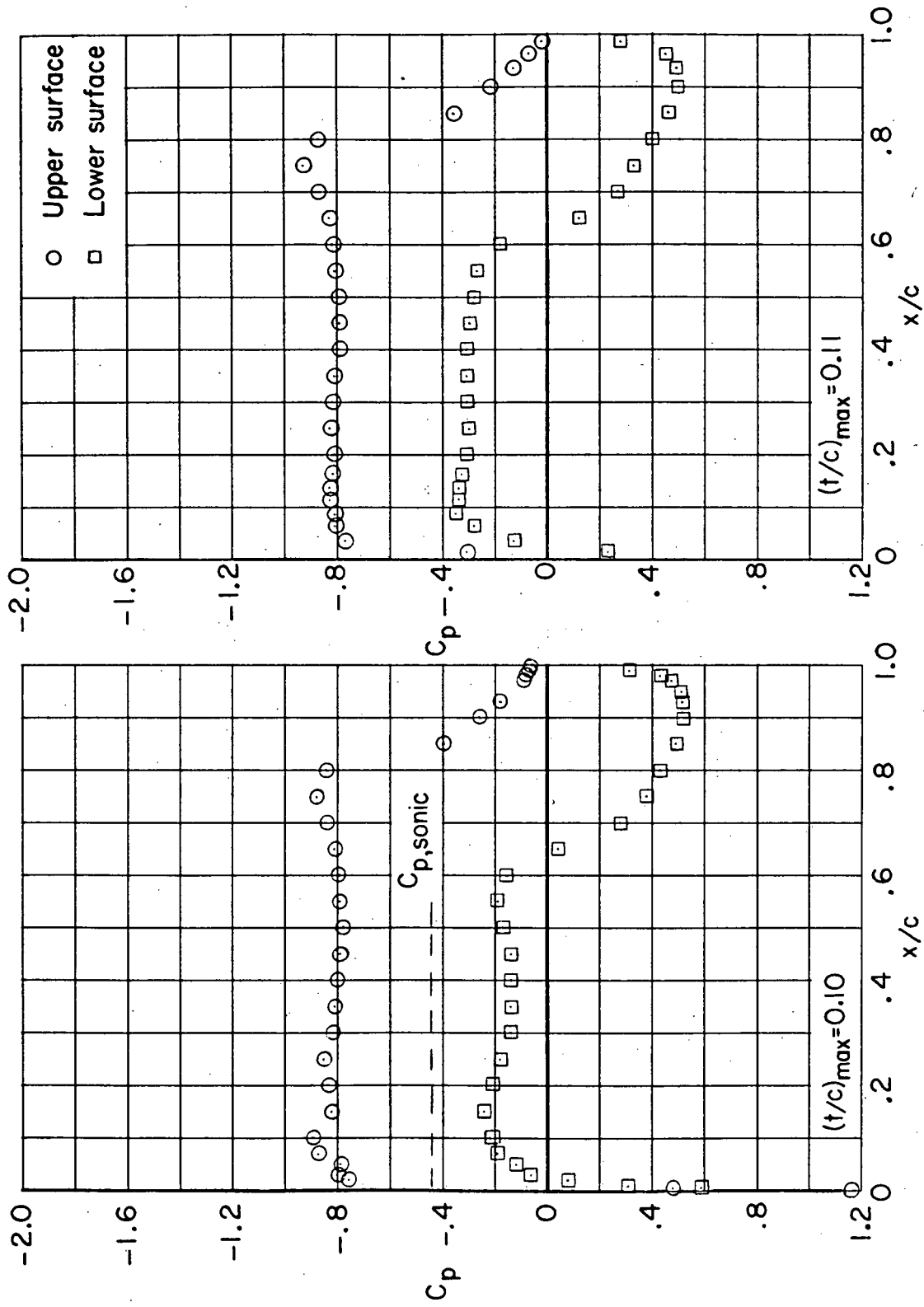


(a) $M = 0.80$; $\alpha = 0.50^\circ$.

Figure 10.- Continued.

~~CONFIDENTIAL~~

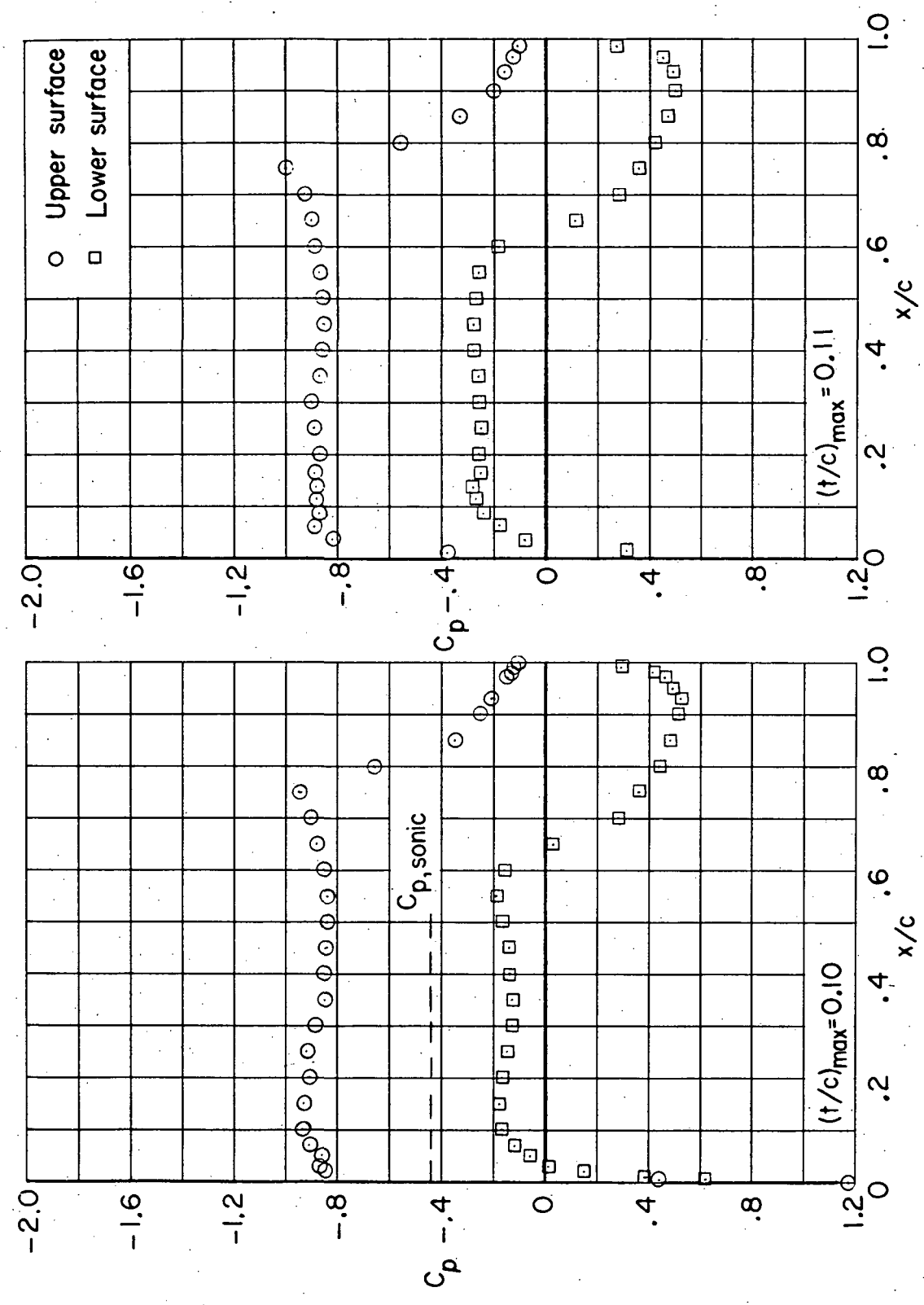
~~CONFIDENTIAL~~



(r) $M = 0.80$; $\alpha = 1.0^\circ$.

Figure 10.- Continued.

~~CONFIDENTIAL~~



(s) $M = 0.80$; $\alpha = 1.5^\circ$.

Figure 10.- Concluded.

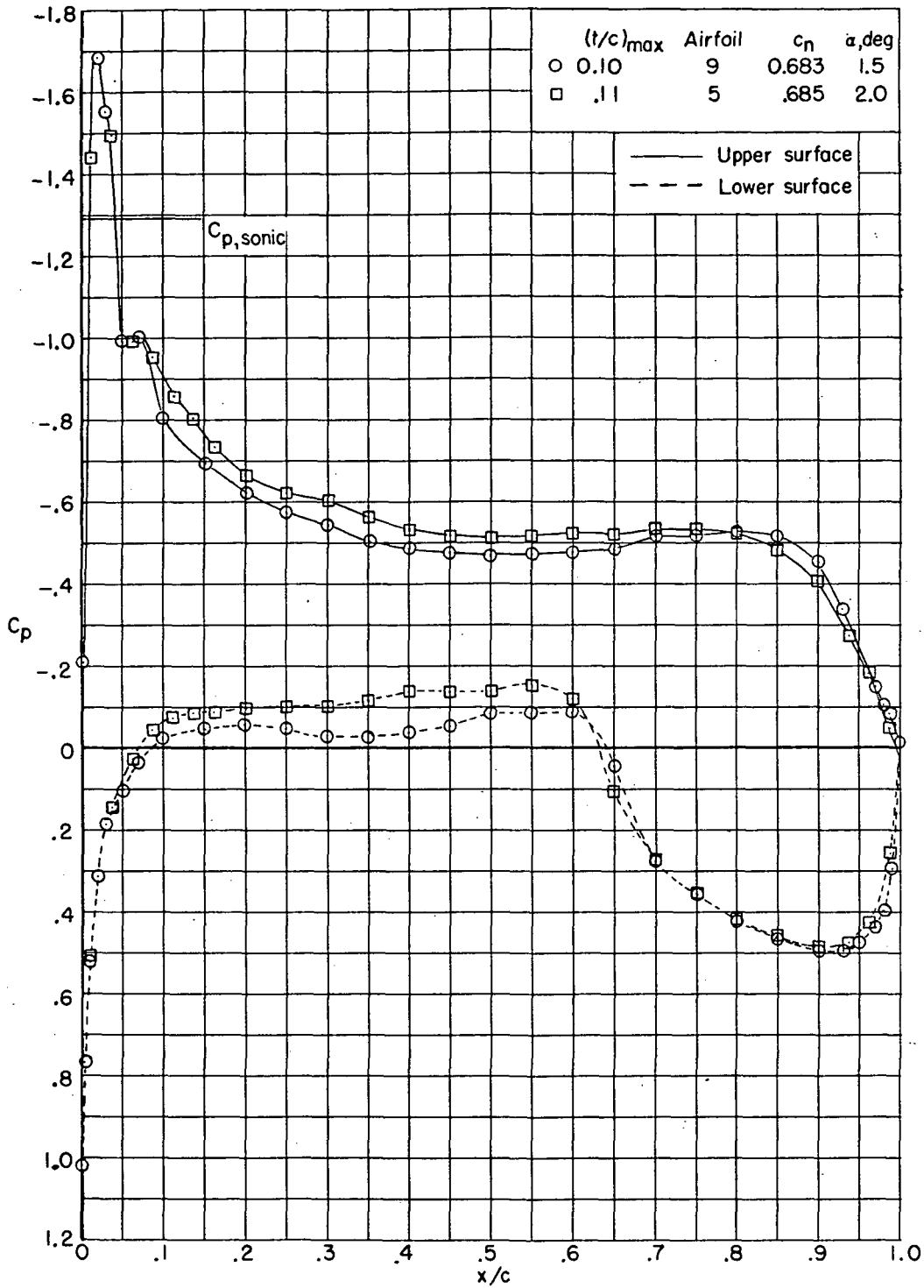


Figure 11.- Chordwise pressure profiles at $M = 0.60$.

~~CONFIDENTIAL~~

~~CONFIDENTIAL~~

~~CONFIDENTIAL~~

"The aeronautical and space activities of the United States shall be conducted so as to contribute . . . to the expansion of human knowledge of phenomena in the atmosphere and space. The Administration shall provide for the widest practicable and appropriate dissemination of information concerning its activities and the results thereof."

— NATIONAL AERONAUTICS AND SPACE ACT OF 1958

NASA SCIENTIFIC AND TECHNICAL PUBLICATIONS

TECHNICAL REPORTS: Scientific and technical information considered important, complete, and a lasting contribution to existing knowledge.

TECHNICAL NOTES: Information less broad in scope but nevertheless of importance as a contribution to existing knowledge.

TECHNICAL MEMORANDUMS: Information receiving limited distribution because of preliminary data, security classification, or other reasons.

CONTRACTOR REPORTS: Scientific and technical information generated under a NASA contract or grant and considered an important contribution to existing knowledge.

TECHNICAL TRANSLATIONS: Information published in a foreign language considered to merit NASA distribution in English.

SPECIAL PUBLICATIONS: Information derived from or of value to NASA activities. Publications include conference proceedings, monographs, data compilations, handbooks, sourcebooks, and special bibliographies.

TECHNOLOGY UTILIZATION PUBLICATIONS: Information on technology used by NASA that may be of particular interest in commercial and other non-aerospace applications. Publications include Tech Briefs, Technology Utilization Reports and Notes, and Technology Surveys.

Details on the availability of these publications may be obtained from:

SCIENTIFIC AND TECHNICAL INFORMATION OFFICE
NATIONAL AERONAUTICS AND SPACE ADMINISTRATION
Washington, D.C. 20546

~~CONFIDENTIAL~~